AFWAL-TR-88-4113

PHASE RELATIONS IN THE Ti_3Al + Nb SYSTEM

Michael J. Kaufman
Assistant Professor
Department of Materials Science and Engineering
FB-10
University of Washington
Seattle, WA 98195

July 1988

Final Report for period of 11 Feb 87 through 15 Oct 87

MATERIALS LABORATORY
AIR FORCE WRIGHT AERONAUTICAL LABORATORIES
AIR FORCE SYSTEMS COMMAND
WRIGHT-PATTERSON AIR FORCE BASE, OHIO 45433-6533

NOTICE

When Government drawings, specifications, or other data are used for any purpose other than in connection with a definitely Government-related procurement, the United States Government incurs no responsibility or any obligation whatsoever. The fact that the Government may have formulated or in any way supplied the said drawings, specifications, or other data, is not to be regarded by implication, or otherwise in any manner construed, as licensing the holder, or any other person or corporation; or as conveying any rights or permission to manufacture, use, or sell any patented invention that may in any way be related thereto.

This report has been reviewed by the Office of Public Affairs (ASD/PA) and is releasable to the National Technical Information Service (NTIS). At NTIS, it will be available to the general public, including foreign nations.

This technical report has been reviewed and is approved for publication.

Charles H. Ward

CHARLES H. WARD, 1LT, USAF
Structural Metals Branch
Metals & Ceramics Division

Gerald Tarnacki

GERALD TARNACKI, CAPT, USAF
Actg Technical Area Manager,
Titanium Group
Structural Metals Branch
Metals & Ceramics Division

FOR THE COMMANDER

FRANCIS H. FROES
Chief, Structural Metals Branch
Metals & Ceramics Division

If your address has changed, if you wish to be removed from our mailing list, or if the addressee is no longer employed by your organization please notify AFWAL/MLLS , Wright-Patterson AFB, OH 45433-6533 to help us maintain a current mailing list.

Copies of this report should not be returned unless return is required by security considerations, contractual obligations, or notice on a specific document.

UNCLASSIFIED
SECURITY CLASSIFICATION OF THIS PAGE

ADA197897

REPORT DOCUMENTATION PAGE

Form Approved
OMB No. 0704-0188

1a REPORT SECURITY CLASSIFICATION Unclassified	1b RESTRICTIVE MARKINGS N/A
2a SECURITY CLASSIFICATION AUTHORITY N/A	3 DISTRIBUTION/AVAILABILITY OF REPORT Approved for public release; distribution is unlimited.
2b DECLASSIFICATION/DOWNGRADING SCHEDULE N/A	
4 PERFORMING ORGANIZATION REPORT NUMBER(S) Univ. of Wash. Report No.	5 MONITORING ORGANIZATION REPORT NUMBER(S) AFWAL-TR-88-4113
6a NAME OF PERFORMING ORGANIZATION Dept. of Mat'ls Sci. & Engr. Univ. of Wash.	6b OFFICE SYMBOL (If applicable)
7a NAME OF MONITORING ORGANIZATION Materials Laboratory (AFWAL/MLLS)	
6c ADDRESS (City, State, and ZIP Code) Wilson Hall, FB-10 Seattle WA 98195	7b ADDRESS (City, State, and ZIP Code) Air Force Wright Aeronautical Labs Wright-Patterson Air Force Base OH 45433-6533
8a NAME OF FUNDING/SPONSORING ORGANIZATION	8b OFFICE SYMBOL (If applicable)
9 PROCUREMENT INSTRUMENT IDENTIFICATION NUMBER F33601 87 M4037	
8c ADDRESS (City, State, and ZIP Code)	10 SOURCE OF FUNDING NUMBERS

PROGRAM ELEMENT NO.	PROJECT NO.	TASK NO	WORK UNIT ACCESSION NO
62102F	2418	02	07

11 TITLE (Include Security Classification)
Phase Relationships in Ti_3Al+Nb System

12 PERSONAL AUTHOR(S)
Kaufman, Michael J.

13a TYPE OF REPORT	13b TIME COVERED	14 DATE OF REPORT (Year, Month, Day)	15 PAGE COUNT
Final	FROM 2/11/87 TO 10/15/87	July 1988	52

16 SUPPLEMENTARY NOTATION

17 COSATI CODES		
FIELD	GROUP	SUB-GROUP
11	6	3
11	6	4

18 SUBJECT TERMS (Continue on reverse if necessary and identify by block number)
Rapid Solidification, Phase Diagram, Titanium, Aluminum, Niobium, Melt Spinning, Splat Quenching, Intermetallic, Metastable.

19 ABSTRACT (Continue on reverse if necessary and identify by block number)

Arc melted buttons, melt spun ribbons and splat quenched foils of various $(TiNb)_3Al$ alloys (up to 30 at. % Nb) have been analyzed in their as-solidified conditions in order to determine the effect of cooling rate on the evolution of non-equilibrium microstructures. For Nb concentrations of 5% and above, the rapidly-quenched structures contained the ordered β-phase (B2 structure) the volume fraction of which was found to increase significantly with both increasing Nb concentration and increasing quenching rate. The structures of these materials were examined carefully using x-ray diffraction and transmission electron microscopy (TEM) and the results indicated that (1) the size of the B2 domains decreased significantly with increasing quenching rate and decreasing Nb concentration, and (2) the B2 phase always displayed "tweed" microstructures and diffraction patterns with considerable diffuse intensity and "extra" diffraction spots, consistent with previous solid-state investigations. In order to investigate the thermal stabilities and decomposition sequences of these microstructures and to generate information concerning the equilibrium phase relationships in this system, the as-solidified microstructures were subjected

20 DISTRIBUTION/AVAILABILITY OF ABSTRACT	21 ABSTRACT SECURITY CLASSIFICATION
☐ UNCLASSIFIED/UNLIMITED ☒ SAME AS RPT ☐ DTIC USERS	Unclassified
22a NAME OF RESPONSIBLE INDIVIDUAL Lt Charles H. Ward	22b TELEPHONE (Include Area Code) (513) 255-1307
	22c OFFICE SYMBOL AFWAL/MLLS

DD Form 1473, JUN 86 Previous editions are obsolete.

SECURITY CLASSIFICATION OF THIS PAGE
UNCLASSIFIED

19. ABSTRACT (continued)

to a series of isothermal heat treatments at temperatures ranging from 800-1250degrees C (1472-2282 degrees F) and examined accordingly. In addition to the isothermal studies, the melt-spun ribbons were also examined by differential thermal analysis (DTA) in an effort to gather further information concerning the phase decomposition sequences in these alloys. The various results will be presented and discussed with reference to the current status of this important class of alloys.

PREFACE

This final report covers the work performed by the University of Washington (UW) under Air Force Contract F33601-87-M4037 for the time period 11 February 1987 through 15 October 1987. The objective of this program was to explore the fundamental phase relationships in a series of Ti-Al-Nb alloys containing 25% Al and from 0-30% Nb (at. pct.). These alloys have been receiving considerable attention as potential high temperature, high specific strength structural materials of importance to the aerospace industries.

This program was conducted within the Department of Materials Science and Engineering at the UW by Assistant Professor M.J. Kaufman with the assistance of graduate research assistants. Much of the work was performed in collaboration with various staff members at AFWAL/MLLS including T. Broderick, Dr. F.H. Froes and Lt. C.H. Ward and their assistance is gratefully acknowledged. In addition, Drs. D.G. Konitzer of Alcoa Technical Center and R.G. Rowe of General Electric Corporate Research and Development Laboratory interacted by supplying materials and through useful technical discussions; their assistance is also gratefully acknowledged. Finally, the expert assistance of Ms. H. Larson in producing this report is highly appreciated.

TABLE OF CONTENTS

LIST OF FIGURES

List of Figures (Continued)

List of Figures (Continued)

1.0 INTRODUCTION

The goal of the present study was to define more accurately the $(Ti_{1-x}Nb_x)_3Al$ phase diagram from 0 to 30 percent Nb under rapid solidification (RS) conditions. The primary reason for choosing RS material had to do with the greater homogeneity of the starting materials compared with that produced by more conventional methods (e.g., nonconsumable arc melting). Unfortunately however, as will be shown below, serious limitations arise when attempting to anneal thin RS material at temperatures above 1000°C (1832°F) due to the significant oxidation that is observed at these temperatures even when precautions are taken to ensure cleanliness. Because of these limitations, bulk samples of three alloys in the composition range of interest were also studied in order to generate data for these higher temperatures.

In order to achieve the program goals, the samples were examined carefully using a variety of characterization methods including thermal analysis, X-ray diffraction, optical and analytical electron microscopy (AEM).

2.0. BACKGROUND

Recently, alloys in the Ti_3Al + Nb system have been receiving considerable attention because of their potential as low-density, high-temperature materials. In fact, a limited number of compositions have been developed and are currently being utilized in applications (e.g., jet turbines). Even so, there remain serious gaps in our understanding of the phase relationships in alloys of this type; this is due, in part, to the lack of any systematic studies of the phase equilibria in this particular system and, as will be shown below, to the complex phase relationships that exist over the composition range of interest.

Before describing the present results, it is instructive to discuss briefly some of the existing data of relevance to this particular system. Banerjee, et al.[1] as well as Stychor, et al.[2] have examined the phase relations in a limited number of Ti-Al-Nb alloys. The former authors concentrated on the issues of β (the high-temperature, disordered bcc phase) and α_2 (the lower temperature, ordered DO_{19} phase) phase transformations for compositions in the vicinity of Ti-25Al-11Nb while the latter examined the decomposition of the metastable B2 phase (CsCl structure) in similar alloys by quenching samples from the β-phase field to room temperature followed by low-temperature anneals. The results of these studies will be discussed below with reference to the data obtained in the present investigation.

3.0 EXPERIMENTAL PROCEDURE

Melt-spun ribbons and splat-quenched foils of the compositions shown in Table 1 were prepared respectively by Dr. R.G. Rowe of GE-CRD and Prof. S.H. Whang of Polytechnic Institute of New York and supplied by Lt. C.H. Ward of AFWAL/MLLS. These materials were analyzed in their as-prepared condition by X-ray diffraction (XRD) and analytical electron microscopy (AEM). Subsequently, sections of the ribbons were cut, cleaned, wrapped in Ta foil, encapsulated in evacuated and He-backfilled quartz tubes, and isothermally heat treated in the range 800-1000°C (1472-1832°F) for times from 5 to 24 hours. Higher-temperature heat treatments were also attempted but the resulting samples appeared oxidized and deformed, indicating that through-thickness oxidation had probably occurred. After heat treatment, the samples (inside quartz tubes) were plunged into salt water and the tubes were broken as quickly as possible in order to enhance the quenching rate and thereby inhibit solid state transformations during the quench. The heat-treated ribbons were then lightly polished, re-examined using XRD and specimens of interest were prepared for examination by AEM.

As will be shown below, the DTA/TMA analyses performed at AFWAL/MLLS on similar melt-spun ribbons indicated that very interesting effects were occurring above 1000°C (1832°F) and that any useful phase diagram assessment must include these higher temperatures. As a result, bulk samples (i.e., arc-melted buttons) of Ti-25Al-20Nb and Ti-25Al-30Nb were obtained from Dr. D.G. Konitzer of Alcoa Technical Center while a third composition, Ti-24Al-11Nb (24-11), was provided by Lt. C.H. Ward of AFWAL/MLLS; this latter alloy had been hot rolled in the "α_2 + B2" phase field followed by air cooling. Sections from these specimens were solution annealed at 1250°C (2282°F) for 4h, water quenched, aged at temperatures between 800 and 1200°C (1472 and 2192°F) for various times and subsequently examined by XRD, optical and analytical electron microscopy.

For the AEM analysis, electron-transport foils were prepared using standard twin-jet polishing procedures and examined in Philips EM 400T, 420, and 430 transmission electron microscopes operating at accelerating voltages from 80 to 300kV.

Table 1. List of RS alloys used in the present study.

Melt-spun ribbons	Splat-quenched foils
Ti-25Al-ONb	
Ti-25Al-5Nb	Ti-25Al-5Nb
Ti-25Al-8Nb	Ti-25Al-8Nb
Ti-25Al-10Nb	Ti-25Al-10Nb
Ti-25Al-12Nb	Ti-25Al-12Nb
Ti-25Al-20Nb	Ti-25Al-20Nb
Ti-25Al-25Nb	Ti-25Al-25Nb
Ti-25Al-30Nb	Ti-25Al-30Nb

4.0 RESULTS

The results of the present study will be presented in 4 sections: (1) as-rapidly solidified structures; (2) DTA/TMA data; (3) heat-treated ribbons; and (4) heat-treated bulk specimens. Subsequently, a phase diagram will be proposed based on the various results.

4.1 As-Rapidly-Solidified Structures

In this section, the results will be presented with an emphasis on displaying the effects of composition and cooling rate on the microstructural evolution of the various alloys.

The as-solidified alloys displayed microstructures which, to some extent, depended on the quenching technique and, in the case of the melt-spun ribbons, the location within the ribbon thickness. For example, XRD and AEM analysis of the 5Nb alloy revealed that the structure of this alloy varied significantly with cooling rate, i.e., for the most rapid cooling rates obtained in the splats, essentially no α (disordered, hexagonal martensite) or α_2 (ordered, hexagonal martensite) was present, whereas in the melt-spun ribbons both α_2 and B2 were observed with the amount of α_2 clearly higher in the thicker regions of the ribbons opposite the surface that was in contact with the wheel (Fig. 1). In addition, the size of the antiphase boundaries (APBs) within the B2 grains was observed to decrease with increasing quenching rate and was somewhat difficult to resolve in the splats (Fig. 2). Consistent with these results was the observation of broader X-ray peaks, indicating a greater degree of disorder, from the splats. Finally, it should be noted that the B2 phase in this and the higher Nb-containing alloys displayed a "tweed" structure (Fig. 3) with corresponding streaking in the selected area diffraction patterns (SADPs). Strychor et al.[2] recently reported similar features in a Ti-27.8Al-11.27 Nb alloy and interpreted the results as consistent with lattice displacement waves of the type $\{110\}\ <1\bar{1}0>$: such lattice distortions result in regions with a pseudo-hexagonal (2H)-type structure. These features have been observed in numerous other alloys (e.g., shape-memory alloys) that exhibit "pre-martensitic" phenomena.[3,4]

Similar results were observed in the 8 Nb alloy except that a lower volume fraction of the α_2 phase was observed for equivalent locations within the ribbons. However, when the Nb concentration was 10 percent or greater, very little if any of the α_2 phase was observed in the rapidly-quenched material (Table 2). Rather, the structures consisted of the ordered B2 phase only. It should be noted that for a given composition, the APB size decreased with increasing quenching rate (Fig. 4) similar, though not as pronounced, to the effect observed for the 5 Nb alloy. In addition, the X-ray peaks were substantially broader in the splats than in the ribbons, consistent with the smaller sizes of the ordered domains and the lower degree of ordering. Finally, as can be seen in Figs. 2, 4 and 5, the size of the ordered domains depends strongly on Nb concentration; as will be discussed below, the increasing domain size with increasing Nb does not seem to support the notion that the effect of Nb is to lower the coarsening kinetics of the ordered B2 domains or that the ordering temperature decreases with increasing Nb. Rather, the results suggest that the temperature of the ordering reaction must be increasing with increasing Nb. It could be argued that the APB sizes in the melt-spun ribbons should vary with location due to the well-documented differences in the solidification rates experienced by different regions within the ribbon (e.g., wheel side vs. air side). However, since the thermal APBs are produced by a solid-state reaction, any such variation is expected to be minimal. Support for this argument was obtained by noting that the B2 peaks in the X-ray patterns taken from opposite sides of the ribbons had similar shapes.

In summary, the present results indicate that the decomposition of the high temperature bcc phase can be suppressed in Ti_3Al containing sufficient levels of Nb by rapid quenching from the liquid state, equivalently, from the β-phase field. Further, the sizes of the "metastable" B2 domains decrease with increasing quench rate and decreasing Nb concentration.

Table 2. Summary of XRD data for the melt spun ribbons and splat-quenched foils before and after heat treatment (HT). The symbol O corresponds to the orthorhombic phase (see Section 4.3). The presence of those phases enclosed in parentheses was inconclusive from the XRD patterns and were identified in the subsequent TEM analyses.

	Atomic Pct. Nb							
	0	5	8	10	12	20	25	30
Ribbons								
Ext. Side	α_2	B2 + α_2	B2 + α_2	B2	B2	B2	B2	B2
Wheel Side	α_2	B2 + α_2	B2 + α_2	B2	B2	B2	B2	B2
Splats	B2	B2	B2	B2	B2	B2	B2	
HT Ribbons								
800°C (1472°F)		α_2	α_2	α_2	α_2(+ O)	O		O
900°C (1625°F)		α_2	α_2	α_2	α_2	O		O
1000°C (1832°F)		α_2	α_2	α_2	α_2(+ B2)	O + B2(+ α_2)		O

4.2 DTA/TMA Results

As mentioned in the experimental section above, the DTA/TMA data for the melt-spun ribbons were generated at AFWAL/MLLS and supplied for examination. First of all, it should be pointed out that the high rates of heating and cooling (50 and 25°C/min, respectively) used to enhance the appearance of the peaks associated with the solid-state phase transformations make it difficult to identify the various phase boundaries with any accuracy. Nevertheless, the information was useful for providing guidance in terms of the temperatures selected for the isothermal heat treatments described below.

DTA

The approximate temperatures at which the various transformations commenced during the DTA experiments are tabulated in Table 3 and plotted in Fig. 6. In addition, representative DTA traces from the 10Nb alloy are shown in Fig. 7. First of all, it is

obvious that, for Nb concentrations ≥8 percent, the metastable B2 structure transforms exothermically during heating, presumably to form equilibrium phases. The temperature at which this transformation commences increases with Nb concentration consistent with the greater stability of the metastable B2 phase containing higher Nb and/or the slower transformation kinetics associated with the presence of Nb. In addition to this relatively large exothermic peak, a smaller exothermic peak was observed at slightly higher temperatures for the ribbons containing 5, 8, 10, and 12 percent Nb. Further heating in the DTA resulted in endothermic peaks for all compositions. These latter peaks are believed to be associated with the nucleation and growth of the ordered B2 phase from the α_2 phase. However, because of the high heating rates employed, it is anticipated that the actual $\alpha_2/\alpha_2 + B2$ phase boundary is somewhat lower than the temperatures given in Table 3. Finally, it should be mentioned that further heating to 1400°C did not reveal sufficient data to suggest a disordering of the B2 phase. This indicates that the disordering temperature is greater than 1400°C or, more likely, that the enthalpy associated with this transformation is insufficient to produce a measurable effect.

Qualitatively, the cooling data (from 1300-1400°C) are consistent with those obtained on heating. For example, upon cooling from high temperatures, an exothermic peak was observed for all of the compositions, as indicated in Table 3, and is consistent with the nucleation and growth of the α_2-phase from the ordered B2 phase. The temperatures associated with this transformation also appear to be consistent with the heating data and provide a lower limit, for the same reasons cited above, of the phase boundary between the single B2 phase field and the two-phase B2 + α_2 field.

TMA

TMA analysis was performed at 10°C/min from room temperature to 800°C (1472°F) on the 10 and 20Nb alloys and the results were reasonably consistent with the DTA data. For the 10Nb alloy, the material began expanding significantly at ~510°C (950°F); this temperature correlates well with the DTA exotherm (onset temperature at 520°C (968°F)) associated with the metastable B2 to α_2 transformation and is consistent with the expansion expected for the B_2 to α_2 transformation. However,

instead of leveling off after the expansion was complete, the specimen began contracting irreversibly (i.e., no corresponding expansion was observed on cooling from 800°C (1472°F)) at ~650°C (1202°F) and continued all the way to 800°C (1472°F).

Table 3. Summary of the DTA data used in Figure 6. The + and - symbols refer to exothermic and endothermic reactions, respectively.

Composition (%Nb)	Heating (°C)	Cooling (°C)
0	1130-	1250+
5	640+ 1110-	1145+
8	510+ 640+ 1080-	1110+
10	520+ 660+ 1050-	1110+
12	580+ 700+ 1050-	poorly defined
20	685+ 820+ 960-	1000+
25	760+ 980-	980+
30	760+ 980-	990+

For the 20Nb alloy, the initial expansion commenced at ~620°C (1148°F) and continued to ~770°C (1418°F). Above this temperature, an irreversible contraction was observed which continued up to the maximum temperature of 800°C (1472°F) and

also during cooling to ~660°C (1220°F) whereupon the curve leveled off. However, a second scan to 800°C (1472°F) resulted in further contraction of the sample.

4.3 Heat-Treated Ribbons

As described in the Experimental section, for heat treatments above 1000°C (1832°F), the samples appeared noticeably oxidized and deformed. Consequently, the analysis was limited to those ribbons heat treated at or below this temperature.

X-ray Diffraction

After annealing, the ribbons were analyzed using XRD and AEM and the results of the former are tabulated in Table 2. For all of the temperatures studied the diffraction patterns displayed many peaks suggesting that the majority phase in the various ribbons after heat treating was either α_2 or the orthorhombic phase (O-phase) with little evidence for the B2 phase except possibly after the 1000°C (1832°F) treatments. These results imply that the phase boundary between the $\alpha_2 + B2$ and the B2 phase fields is above 1000°C (1832°F) for all of the compositions studied but says little about the lower-temperature phase boundaries--these latter boundaries will be discussed in a later section.

Analytical Electron Microscopy

Because of the large number of alloy compositions available, it was decided initially to analyze the 5, 12, 20 and 30 Nb alloys after heat treating. For the 5 Nb alloy at 800°C (1472°F) and 900°C (1652°F), the microstructure appeared to be single phase (Fig. 8). Convergent-beam electron diffraction (CBED) was used to analyze the structure of this phase and the results were consistent with the hexagonal α_2 phase. However, after heat treating at 1000°C (1832°F) for 5h the microstructure appeared to contain a very small volume fraction of the B2 phase located primarily at grain-boundary triple points (Fig. 9). This suggests that the phase boundary between the α_2 and $\alpha_2 + B2$ fields lies slightly below 1000°C (1832°F) for this composition.

Fig. 10 displays the microstructure and corresponding SADP from the 12 Nb ribbon after heat treating for 5 h at 800°C (1472°F). At can be seen in this figure, the structure appears similar to that shown recently by Banerjee et al.,[1] thereby suggesting that the α_2 phase underwent a phase separation reaction to produce a mixture of the α_2 and orthorhombic phases.

In order to gain further insight into the nature of this apparent orthorhombic phase, single phase regions in 12, 20 and 30 Nb alloy ribbons were examined using CBED. Convergent-beam patterns (CBPs) from the zone parallel to $[0001]_{\alpha_2}$ are shown in Fig. 11. From these CBPs, it is clear that the projection-diffraction and whole-pattern symmetries are both *2mm* (using the notation of Buxton, et al.[5]) implying that the diffraction group is either *2mm* or $2\,mml_R$. Further, when "$11\bar{2}0$-like" poles from this phase were examined by CBED, it was found that they all displayed projection-diffraction symmetries of *2mm*, while some differences were observed for the whole-pattern symmetries, i.e., some had *2mm* symmetry while others had only a single mirror in the whole pattern (Fig. 12). This implies that the diffraction group for the CBP with the *2mm* whole-pattern symmetry is $2\,mml_R$ or *2mm* while that for the CBP with *m* whole pattern symmetry is 2_Rmm_R. Similar results were obtained when the "$1\bar{1}00$-like" poles were examined (e.g., Fig. 13). By taking these various results into consideration and employing the tables in Ref. 5, it can be shown that the only consistent point group is *mmm*. The lattice parameters corresponding to this structure are a$\sim$0.62 nm, b$\sim$0.94 nm and c$\sim$0.47 nm. Though Banerjee, et al.[1] also concluded that the point group of this phase in a 12.5 Nb alloy was *mmm*, their lattice parameters were significantly different (a=0.519nm, b=0.678nm and c=1.107nm).

Because there are 28 possible space groups with the *mmm* point group, it is useful initially to determine the nature of the unit cell by projecting the reflections in the higher order Laue zones into the zero layer. This is accomplished most readily by considering the 100-type poles which have $2mml_R$ diffraction groups. When this is done for the 010 pole (Fig. 13), it becomes clear that the Bravais lattice is not primitive but rather is consistent with a based-centered orthorhombic lattice in real space.

The next step in the space group analysis is to determine the presence of any symmetry elements (glide planes and/or screw axes) since these elements typically result

in the presence of "bars" of zero intensity (dynamic absences, Gjonnes-Moodie lines, etc.) in kinematically-forbidden reflections where intensity has been generated by dynamic (double) diffraction.[6] When the 100 CBP in Fig. 12 is examined more closely, it becomes clear that the $00\ell(\ell = 2n + 1)$ reflections contain dynamic absences. This result implies the existence of both a [001] two-fold screw axis and a (010) glide plane.[6] By combining this information with that given above, it can be concluded that the only consistent space group is *Cmcm* in agreement with the analysis of Banerjee, et al.[1]

4.4 Bulk Samples

As mentioned previously, because oxygen contamination of the ribbons appeared to have occurred during the high-temperature exposures and/or subsequent water quench, bulk samples of 25 Al-20 Nb, 25 Al-30 Nb and 24 Al-11 Nb (24-11) were chosen for examination. The first two alloys were prepared by non-consumable arc melting (supplied by Dr. D.G. Konitzer of Alcoa) while the latter was supplied after being extruded in the $\alpha_2 + B2$ phase field by Lt. C.H. Ward of AFWAL/MLSS. Sections from the various alloys were solution treated at 1250°C (2282°F) for 4 h, water quenched and then isothermally annealed at temperatures between 800 and 1200°C (1472 and 2192°F) for times ranging from 4 to 24 h followed by water quenching.

X-ray Diffraction

After heat treatment, the various sections were polished and then examined using XRD. Before describing the results however, it should be mentioned that the majority of the samples examined contained large grains and, therefore, were appropriate for qualitative analysis only. Nevertheless, the results are informative because it is relatively easy to distinguish between specimens which contain the bcc phase only and those which contain either the α_2 or the orthorhombic phase. Unfortunately however, since most of the α_2 peaks overlap with peaks from the O-phase, it is difficult to ascertain the presence of α_2 when a substantial volume fraction of the O-phase is present. The other problem with analyses of this type is the fact that the phases present at the elevated temperatures are not necessarily retained during the quench and, therefore,

the XRD data must be correlated carefully with the results from the other analyses. In any case, the XRD data are tabulated in Table 4 and will be utilized to help substantiate the results of the optical and AEM analyses presented below.

Table 4. Summary of XRD data for the bulk samples after the various heat treatments listed. The presence of those phases listed in parentheses was inconclusive from the XRD patterns but were identified in the TEM analyses.

Temperature	Composition Ti-24Al-11Nb	Ti-25Al-20Nb	Ti-25Al-30Nb
800°C (1472°F)	α_2	O(+α_2)	O(+α_2)
900°C (1652°F)	α_2(+B2)	O(+α_2)	O(+α_2)
1000°C (1832°F)	α_2 + B2	α_2 + B2(+O)	O(+α_2 + B2)
1050°C (1922°F)	α_2 + B2		
1100°C (2012°F)	α_2 + B2	α_2 + B2(+O)	α_2 + O + B2
1150°C (2102°F)	α_2 + B2	α_2 + B2	B2(+α_2 + O)
1200°C (2192°F)	B2	B2	B2
1250°C (2282°F)	α_2 + B2	B2	B2

Optical and Analytical Electron Microscopy

As mentioned above, the bulk samples were examined by optical and analytical electron microscopy in order to provide complementary data concerning the phase equilibria of the various alloys as a function of temperature and composition.

Ti-24Al-11Nb

Fig. 14 displays the results for the 24-11 alloy. First of all, the microstructure after heat treating a sample at 1250°C (2282°F) for 5 h and water quenching suggests that the structure was single phase at this temperature and transformed during the water quench presumably because of a relatively slow quenching rate. This is consistent with

the XRD results which indicated that the microstructure was not 100 percent B2 but contained a significant fraction of α_2.

The sample heat-treated at 1200°C (2192°F), on the other hand, appeared to be single-phase B2 in the optical micrograph (Fig. 14b) consistent with the XRD data in Table 4. AEM analyses of heat-treated specimens also indicated that the structure was single-phase B2. Further, the similarity in the size of the antiphase domains (Fig. 15) to those observed in the melt-spun ribbons of slightly different compositions, suggests that the structure of this alloy at 1200°C (2192°F) was disordered bcc and that ordering occurred during the water quench.

Samples reheated to temperatures between 1000 and 1150°C (1832 and 2102°F) for 4h contained large precipitates at grain boundaries and in the matrix (Fig. 14). AEM analyses of the second phase in these alloys was consistent with the hexagonal α_2 structure instead of that of the O-phase (Fig. 16). Finally, for samples annealed at 800 and 900°C (1472 and 1652°F), it is clear that the volume fraction of the α_2 phase increases with decreasing temperature (Fig. 14 and 17). Unfortunately, it is difficult to establish conclusively the temperature of the α_2/α_2+ B2 phase boundary based on observations such as these where equilibrium may not have been achieved during the 24h anneals. It is interesting to note, however, that the DTA data imply that this phase boundary is less than 1050°C (1922°F) though almost certainly above 900°C (1652°F).

Ti-25Al-20Nb

For the 20 Nb alloy, the optical micrographs in Fig. 18 indicate that the B2/B2 + α_2 phase boundary lies somewhere between 1150 and 1200°C (2102 and 2192°F). This result is supported by the XRD and AEM analyses: for samples heat-treated at 1000 and 1100°C (1832 and 2012°F), the AEM analysis revealed that the matrix was B2 with laths of α_2, some of which had decomposed to the O-phase (Fig. 19) in a manner similar to that observed for the 12 Nb ribbon at 800°C (1472°F) (Fig. 10). At 900°C (1652°F) the structure appeared to contain a very small fraction of B2 as can be seen in the backscattered electron image in Fig. 20. This implies that the boundary between the O (or O + α_2) and O + B2 (or O + B2 + α_2 phase fields lies slightly below 900°C (1652°F) for this composition. The XRD data were consistent with this analysis:

the peaks corresponding to the B2 phase decreased with decreasing annealing temperature and were weak or nonexistent after the 800 and 900°C (1472 and 1652°F) anneals.

Ti-25Al-30Nb

The optical micrographs (Fig. 21), XRD data and AEM results from the 30 Nb alloy were similar to those just described for the 20 Nb alloy suggesting that the $B2/B2+\alpha_2$ and the $B2+O/O$ phase boundaries are in the range 1150 to 1200°C (2102 to 2192°F) and 900 to 950°C (1652 to 1742°F), respectively. It should be mentioned that the intensities of the superlattice reflections in SADPs obtained from the B2 phase in the 20 and 30 Nb alloys after heat treatment were significantly lower than those obtained from the lower Nb concentrations after similar heat treatments (Fig. 22). Initially, it was speculated that these lower intensities were caused by a greater degree of disorder at the higher Nb concentrations. However, when the SADPs were compared with those obtained from the melt-spun ribbons, it became clear that the superlattice intensities were substantially higher in the latter indicating that this explanation is invalid. This is supported by the fact that the domain size in the heat-treated materials (Fig. 23) was substantially larger than that in the rapidly-quenched specimens. Thus, the lower superlattice intensities must be associated with a greater degree of order in the B2 phase. Because of the different atomic scattering amplitudes of the three elements, this can only be valid if, after annealing, the Nb and Al tend to occupy one sublattice and Ti the other. This result is consistent with the analysis of Banerjee, et al.[5] who utilized channeling-enhanced microanalysis to study site occupation in the B2 phase of a Ti-25Al-10Nb alloy and determined that Nb preferentially occupied the Al sublattice.

5.0 DISCUSSION

The various results reported above can be utilized to make some speculations concerning the phase relationships in the Ti_3Al + Nb system. However, because of the complexities encountered, it is clear that more experimental work must be done to refine the phase boundaries proposed below.

5.1 β/B2 Phase Boundary

The results from the rapidly-quenched alloys indicate that the ordering temperature for the B2 phase increases with Nb concentration. This is based on the fact that the antiphase domains increase in size as the Nb concentration is raised from 0 to 30 percent for similar quenching rates. The effect is most noticeable at the lower Nb concentrations and less so above 20 Nb which may indicate that the phase boundary becomes flatter at the higher Nb contents. Alternatively, the similarities at the higher Nb concentrations may reflect the lower coarsening rates associated with increasing Nb.[8] In any case, it is evident that further work (e.g. higher temperature anneals) must be performed to substantiate these speculations.

5.2 B2/B2 + α_2 Phase Boundary

By combining the various data presented above, it is possible to speculate on the location of the B2/B2 + α_2(or α) phase boundary. Unfortunately, because of the high temperatures associated with this boundary and the fact that bulk samples of the 5 Nb alloy were not studied, it was not possible to determine the location of the boundary for this composition. Even so, by taking into consideration the approximate location of the β-transus for the Ti_3Al composition and the B2/B2 + α_2 boundary for the 24-11 alloy, it is possible to speculate on the approximate location for the 5 Nb concentration as will be shown below.

From the optical microscopy data described above, it appears that all three bulk alloys are single-phase B2 at 1200°C (2192°F) and two-phase α_2 + *B2* at 1150°C

(2102°F). This indicates that the location of the phase boundary of interest is somewhere between these temperatures for Nb concentrations from 11 to 30 percent Nb. This result suggests that the location of this phase boundary is not a strong function of Nb concentration as suspected initially.

5.3 $\alpha_2/\alpha_2 + B2$ Phase Boundary

The location of this particular phase boundary as a function of Nb is much more speculative than that for the $B2/B2+\alpha_2$ phase boundary described above. This is further complicated by the fact that the higher Nb alloys (>11 Nb) also undergo a transformation to the O-phase indicating that there are regions on the phase diagram where all 3 phases (α_2+B2+O) co-exist in equilibrium as well as a two-phase field corresponding to the α_2+O phases. For example, in the 20 Nb alloy heat treated at 1100°C (2012°F), all three phases were observed; even so, the fact that the O-phase was forming by the decomposition of the α_2 may indicate that equilibrium had not been reached during the heat treatment.

Regardless of the complexities mentioned above, the current results do allow us to draw a boundary which represents the temperature below which no B2 is observed. For example, it was shown that there exists a very small volume fraction of B2 in the 5 Nb ribbon after heat treating for 5 h at 1000°C (1832°F) suggesting that the phase boundary is slightly below 1000°C (1832°F) for this particular composition. Similarly, the higher volume fraction of the B2 phase in the 24-11 alloy at 1000°C (1832°F) indicates that this phase boundary is at a lower temperature though still above 900°C (1652°F). Finally, for the 20 and 30 Nb alloys, it was shown that the boundary of interest was somewhere near 900°C (1652°F) for the 20 Nb alloy and between 900 and 950°C (1652 and 1742°F) for the 30 Nb alloy. Again, careful studies of alloys held at temperatures in these ranges will be necessary to refine the location of this particular phase boundary.

6.0 CONCLUSIONS AND RECOMMENDATIONS

A variety of methods and materials have been utilized in an attempt to characterize experimentally the phase relationships in Ti_3Al + Nb alloys. The various results suggest, first of all, that the ordering temperature of the bcc phase increases with increasing Nb concentration. Secondly, the data indicate that the boundary between the ordered B2 and the B2 + α_2 phase fields does not decrease precipitously as suspected initially; in fact, the present results suggest that this boundary is almost flat (between 1150 and 1200°C (2102 and 2192°F)) over the composition range 10-30 percent Nb. Finally, it was shown that the location of the lower temperature phase boundary, below which no B2 is present, is approximately 990°C (1814°F) for the 5 Nb alloy and decreases gradually to temperatures between 900 and 950°C (1652 and 1742°F) for the 30 Nb composition. These various results are summarized in the phase diagram drawn in Fig. 24. Unfortunately, not enough data have been generated to allow us to draw these boundaries more accurately or to draw the boundaries corresponding to the phase fields containing the O and α_2 phases; further investigation is clearly necessary to define these boundaries with greater accuracy.

REFERENCES

1. Bannerjee, D., Gogia, A.K., Nandi, T.K. and Joshi,V.A., "A New Ordered Orthorhombic Phase in a $Ti_3Al + Nb$ Alloy," (preprint).

2. Strychor, R., Williams, J.C. and Soffa, W.A., "Phase Transformation and Modulated Microstructures in Ti-Al-Nb Alloys," (preprint).

3. Otsuka, K., Kubo, H. and Wayman, C.M., "Diffuse Electron Scattering and 'Streaming' Effects," *Met. Trans.*, vol. 12A, pp. 595-605, April 1981.

4. Wen, S.H., Khatchaturyan, A.G., and Morris, J.W. Jr., "Computer Simulation of a 'Tweed-Transformation' in an Idealized Elastic Crystal," ibid., pp. 581-587.

5. Buxton, B.F., Eades, J.A. Steeds, J.W. and Rackham, G.M., "The Symmetry of Electron Diffraction Zone Axis Patterns," *Phil. Trans. R. Soc. London*, vol. A281 pp. 171-194, March 1976.

6. Eades, J.A., Shannon, M.D. and Buxton, B.F., "Crystal Chemistry from Electron Diffraction," (preprint).

7. Bannerjee, D., Nandi, T. and Gogia, A.K. "Site Occupation in the Ordered Beta Phase of Ternary Ti-Al-Nb Alloys," *Scripta Met.*, vol. 21 (1987) pp. 597-600.

8. Sastry, S.M.L. and Lipsitt, H.A., "Ordering Transformations and Mechanical Properties of Ti_3Al-Nb Alloys," *Met. Trans.*, Vol. 8A, pp. 1543-1552, October 1977.

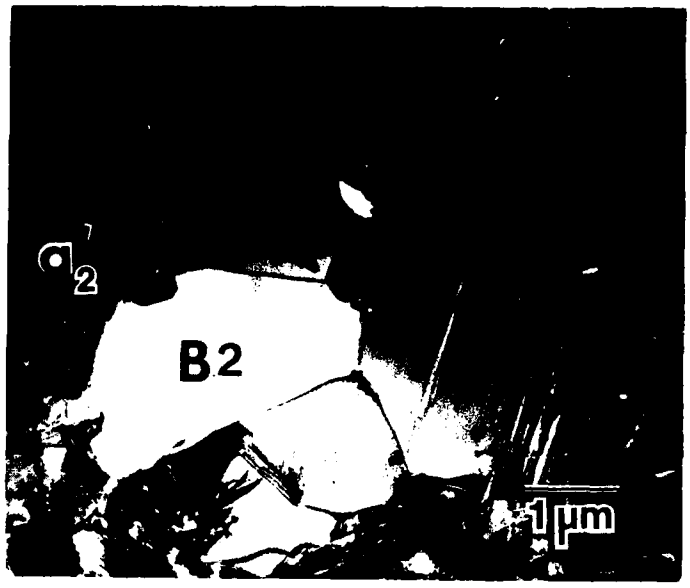

a

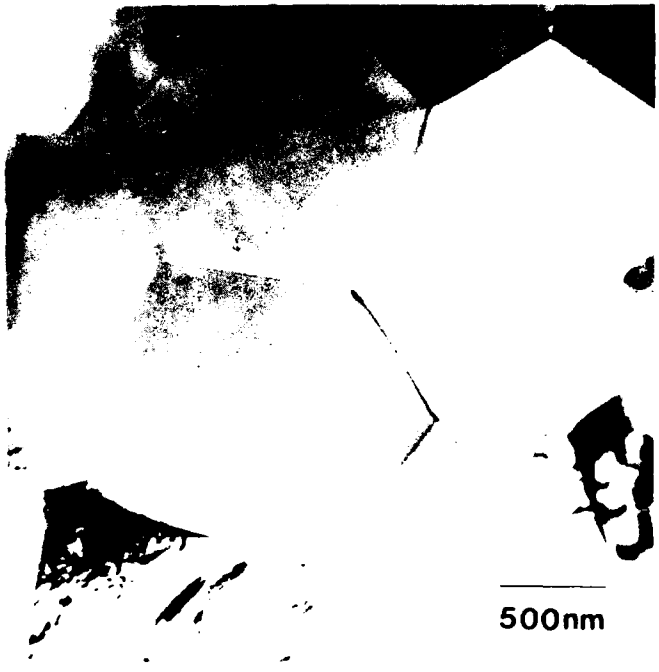

b

Figure 1 Bright field transmission electron micrographs (BFTEM's) of the Ti_3Al+5Nb alloy. (a) melt-spun ribbon, (b) splat-quenched foil.

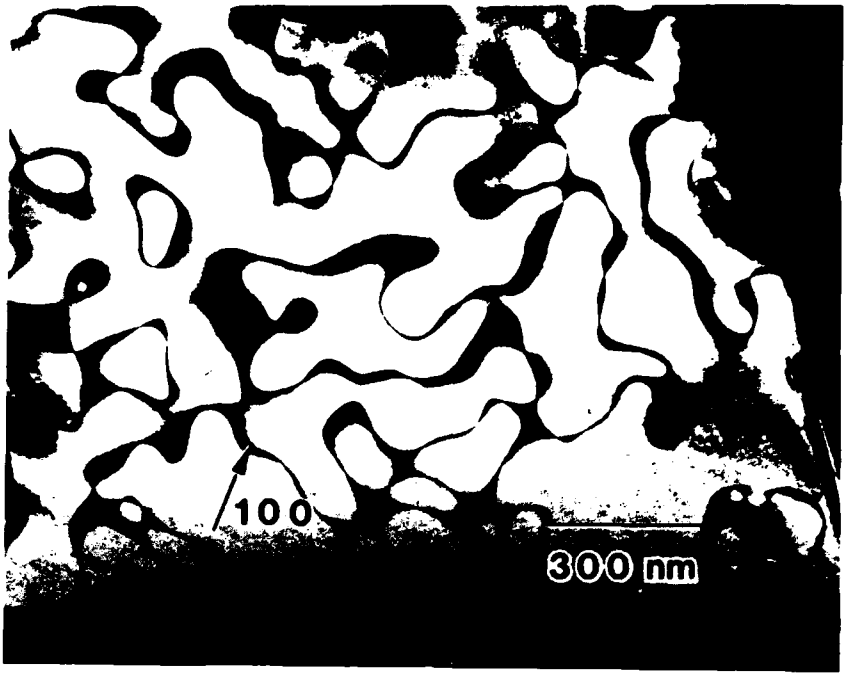

a

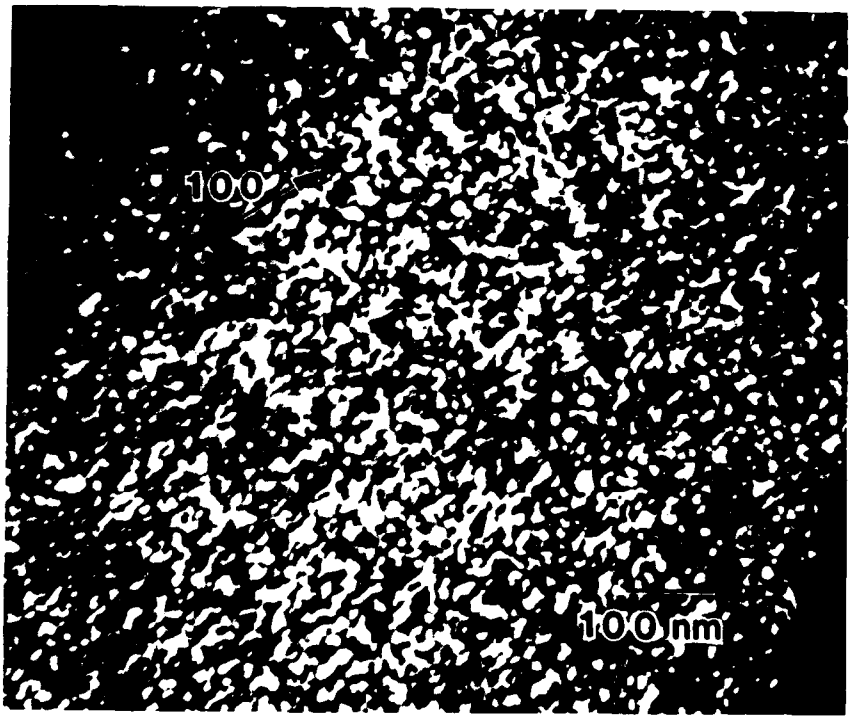

b

Figure 2 Dark field transmission electron micrographs (DFTEM's) of the 5Nb alloy. (a) melt-spun ribbon; (b) splat-quenched foil.

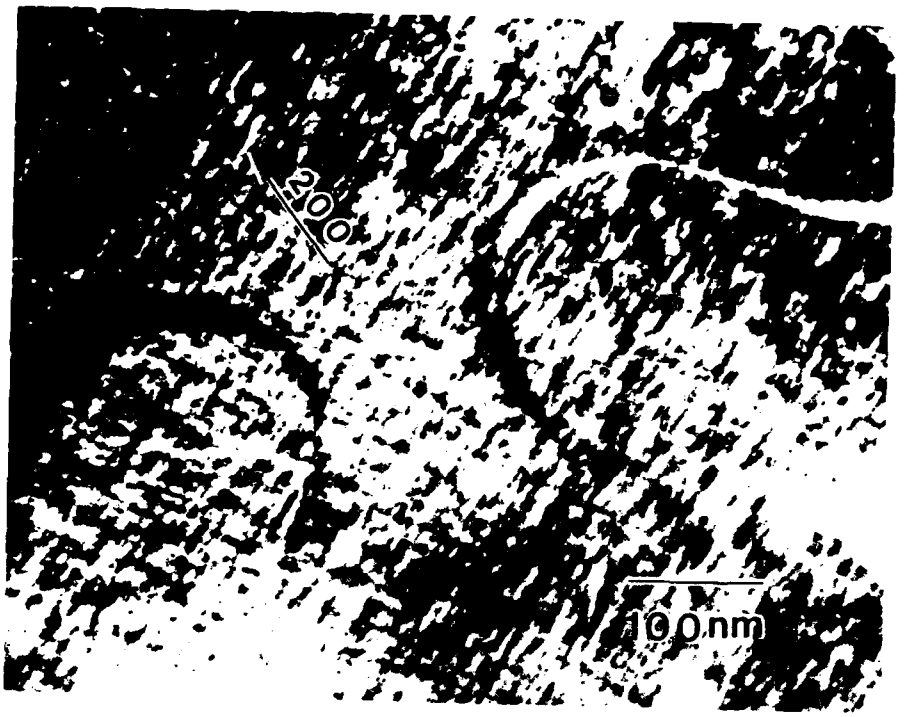

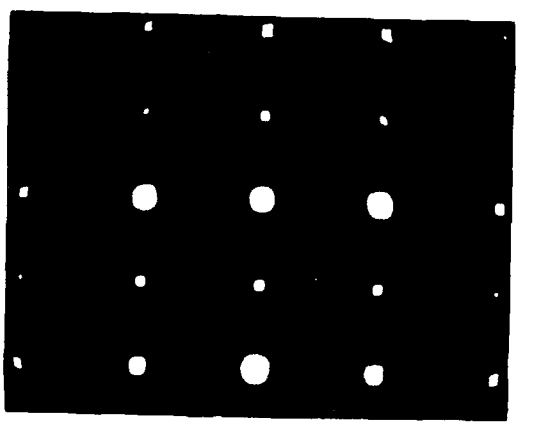

Figure 3 BFTEM and SADP (B=[011]) of a B2 grain in the 8Nb ribbon. The presence of the "tweed" structure and corresponding streaking in the SADP should be noted

a

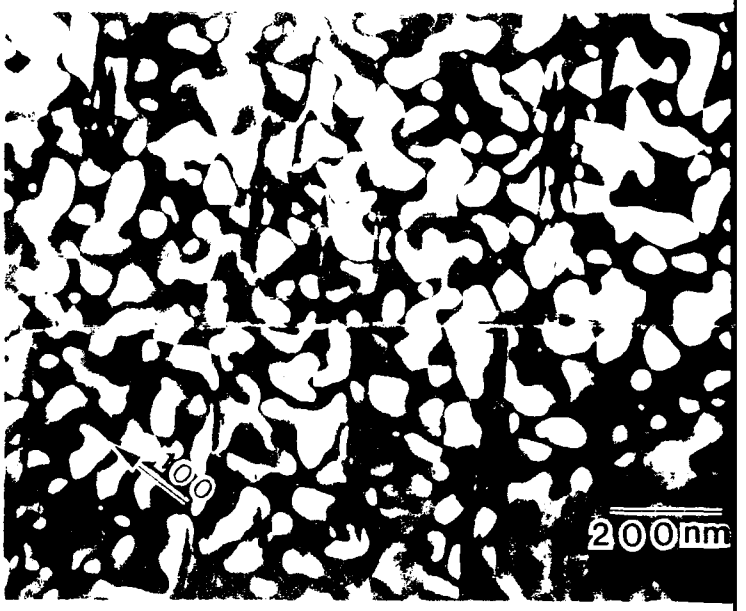

b

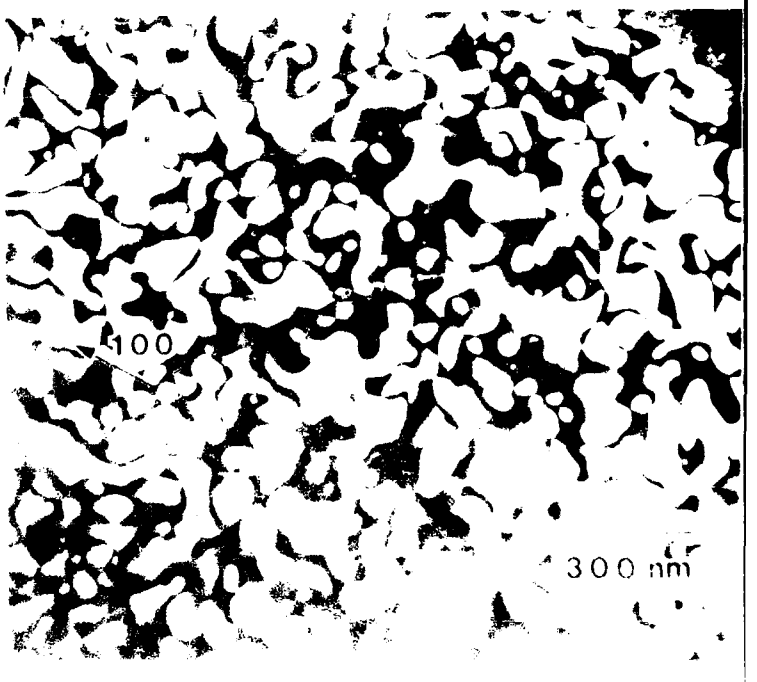

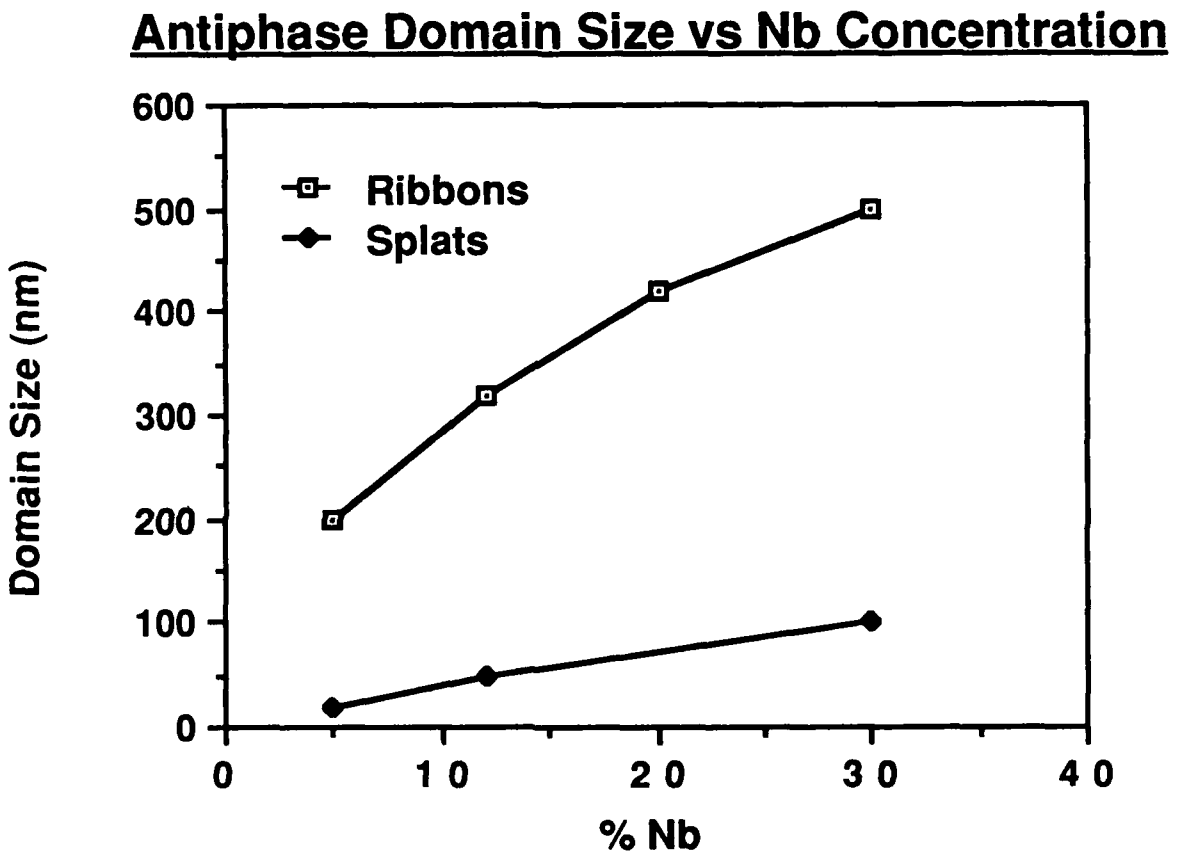

Figure 5 Approximate APB size vs composition for the melt-spun ribbons and splat-quenched foils.

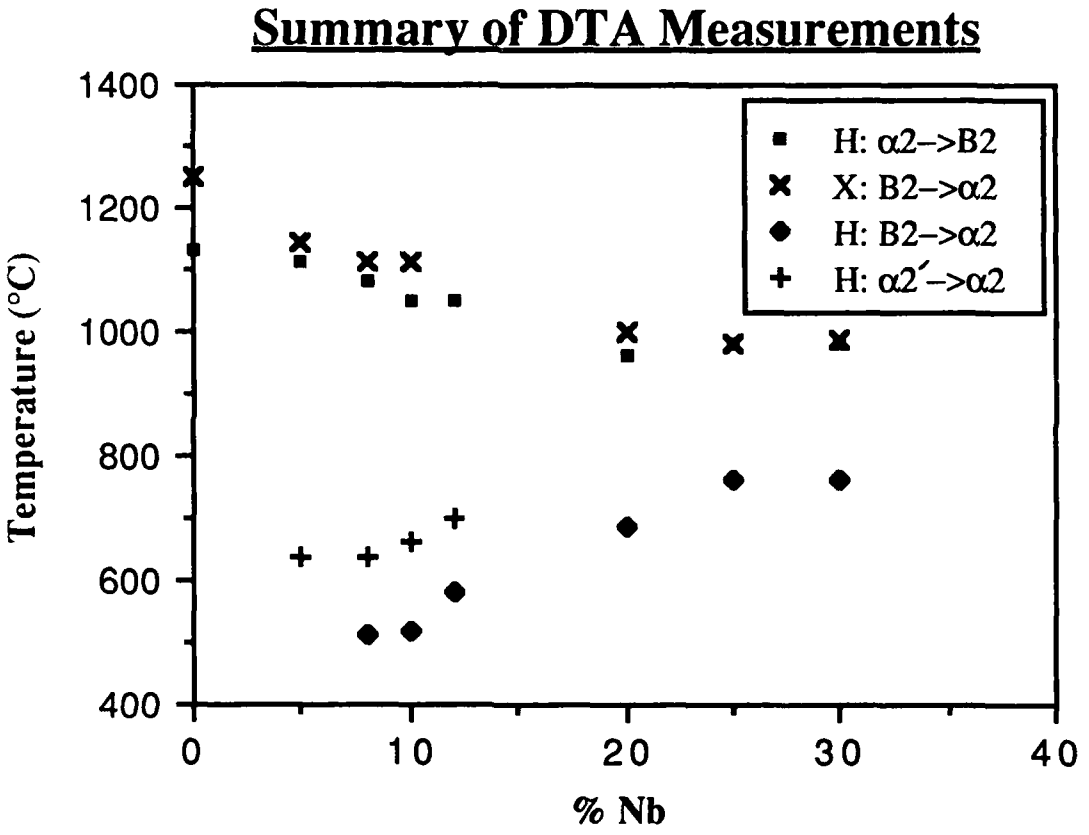

Figure 6 Temperature-composition diagram with the locations of the onsets of the endothermic and exothermic peaks indicated (see Table 3). In the legend H and C refer to heating and cooling, respectively.

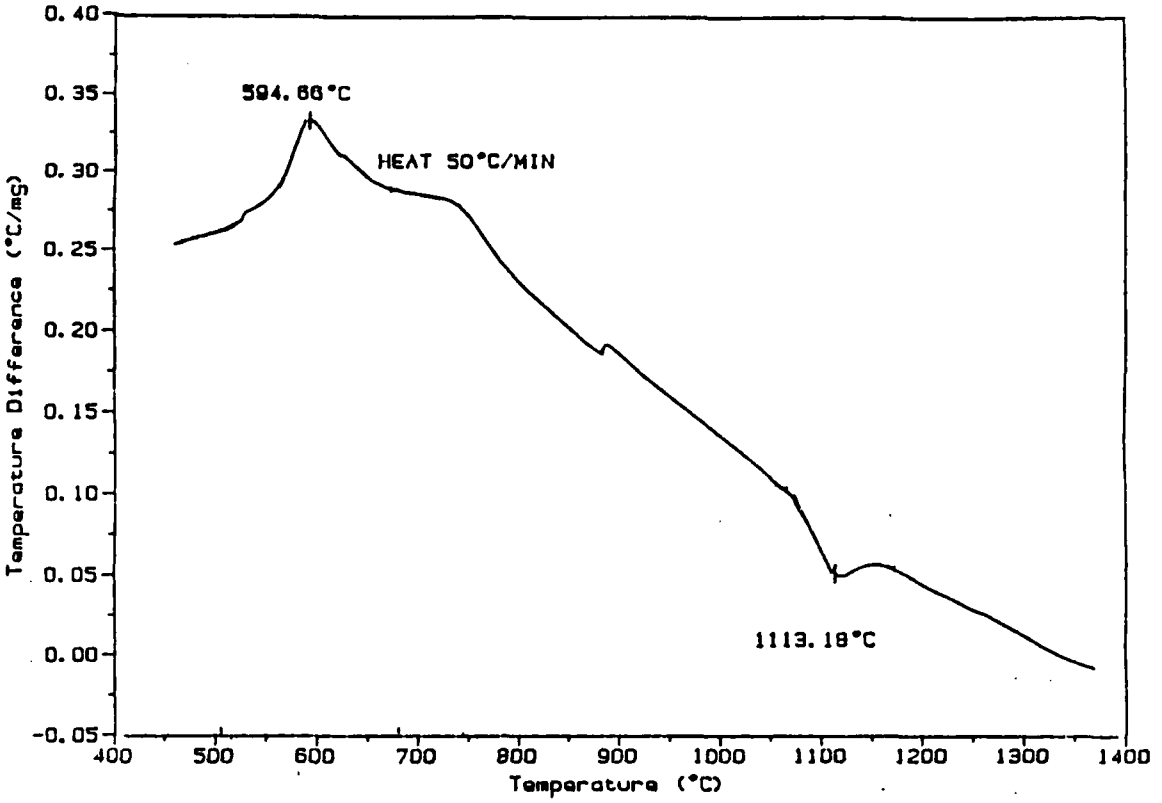

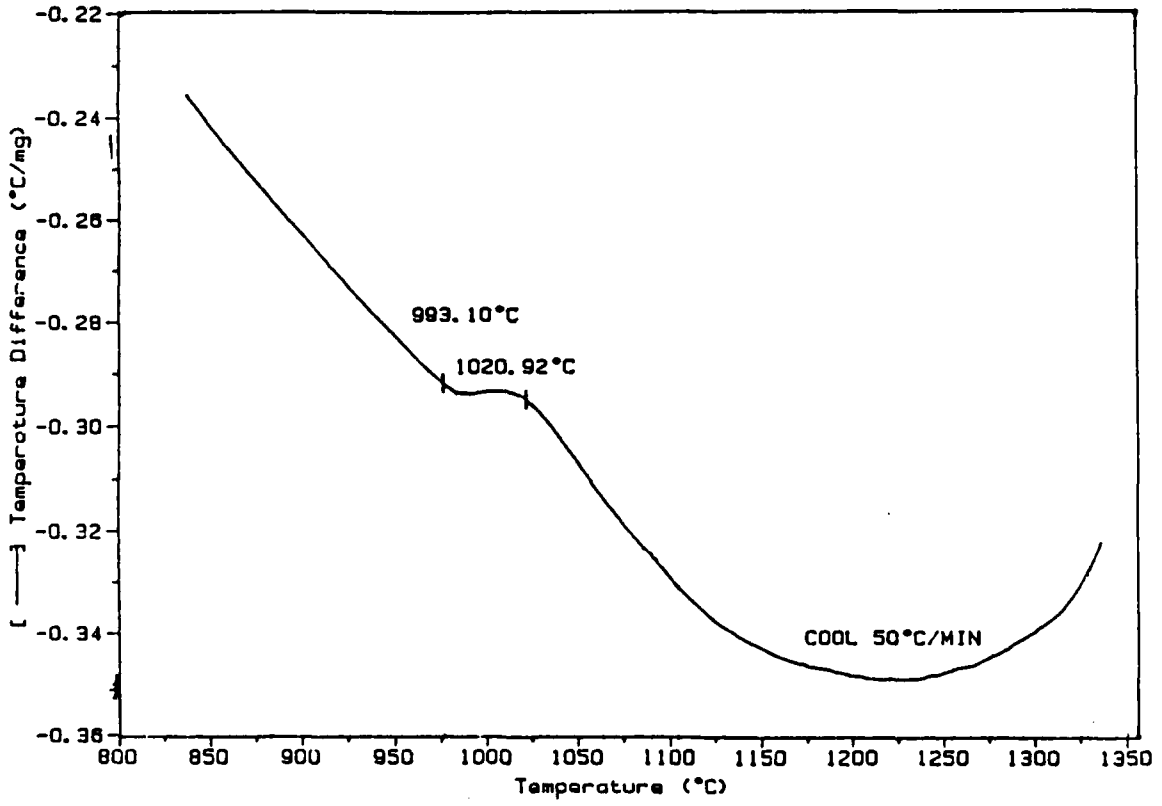

Figure 7 DTA heating and cooling traces from the 10 Nb ribbon displaying the "typical" features described in the text.

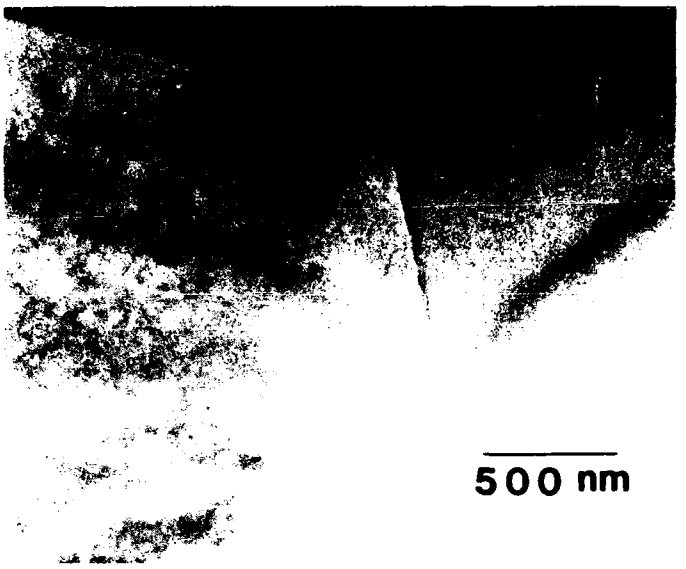

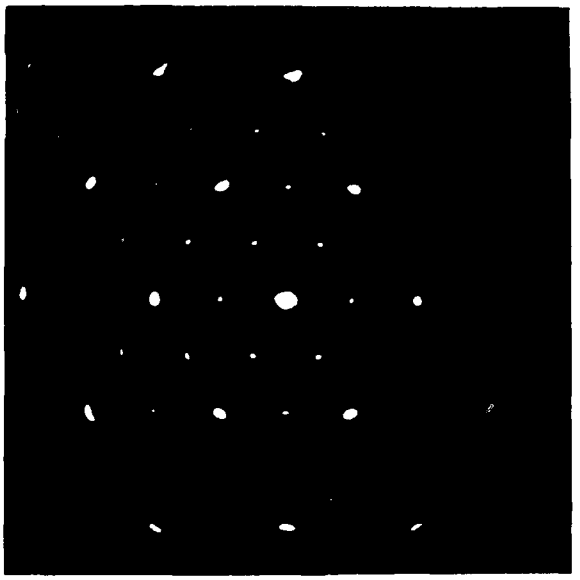

Figure 8 BFTEM and SADP of 5Nb ribbon after annealing at 900°C (1472°F) for 5h. The SADP is consistent with the [0001] zone axis of the α_2-phase.

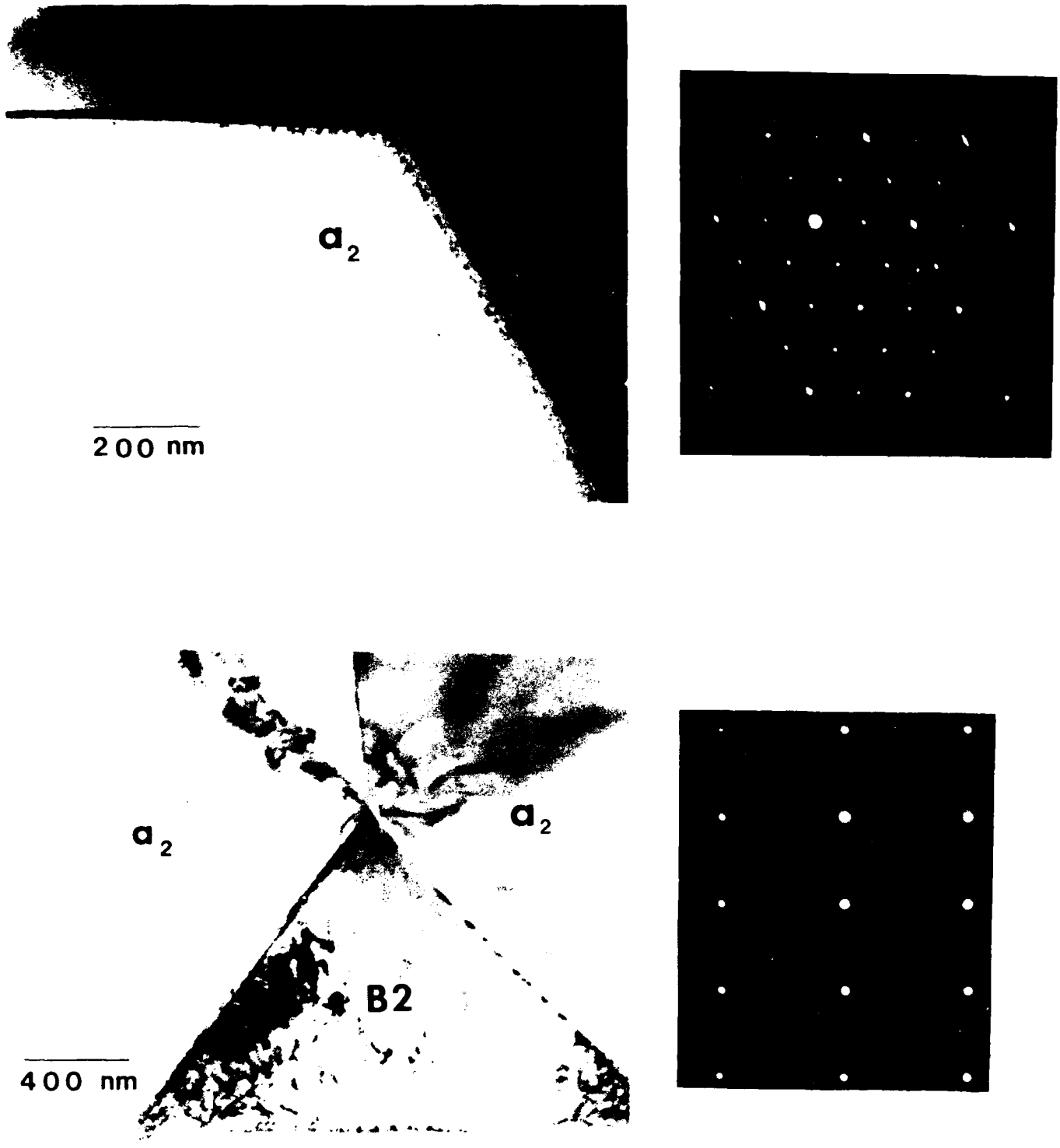

Figure 9 BFTEMs of a 5Nb ribbon after annealing at 1000°C (1832°F) for 5h. Though most of the material was α_2, a small amount of the B2 phase was observed, particularly at grain boundary triple points.

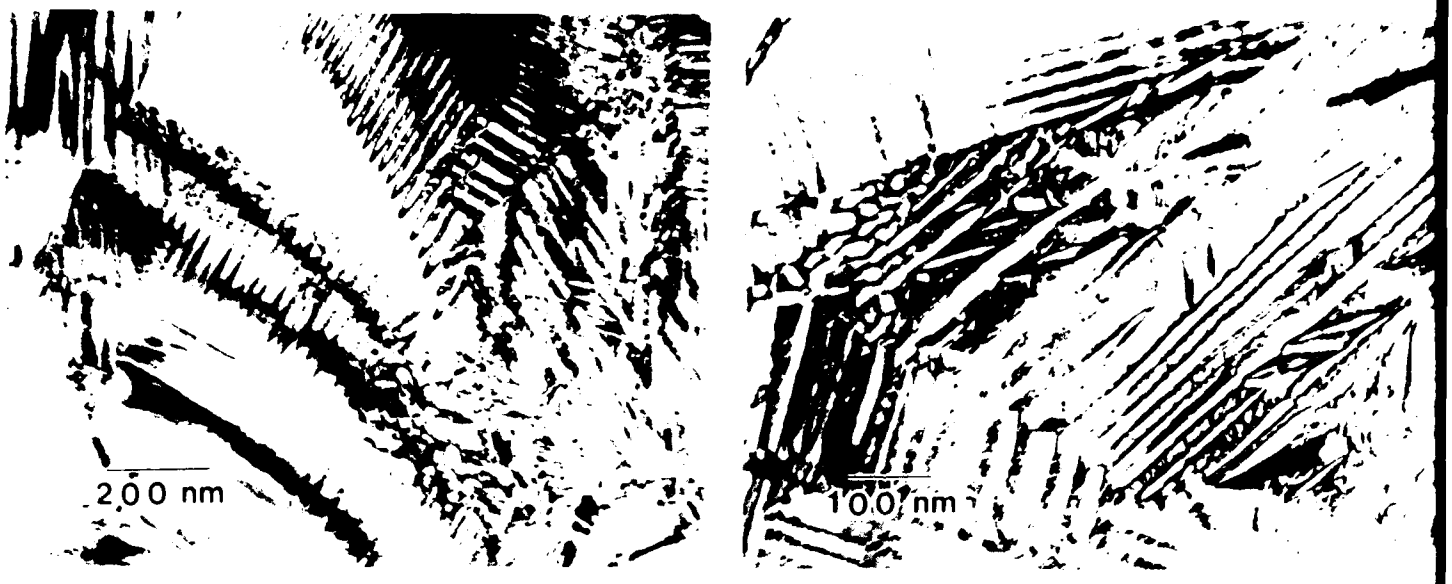

a

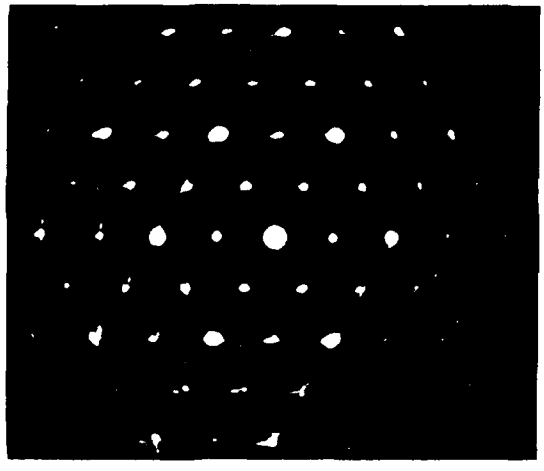

b

Figure 10 (a) BFTEMs and (b) SADP of a 12Nb ribbon after annealing for 5h at 800 C (1473 F).

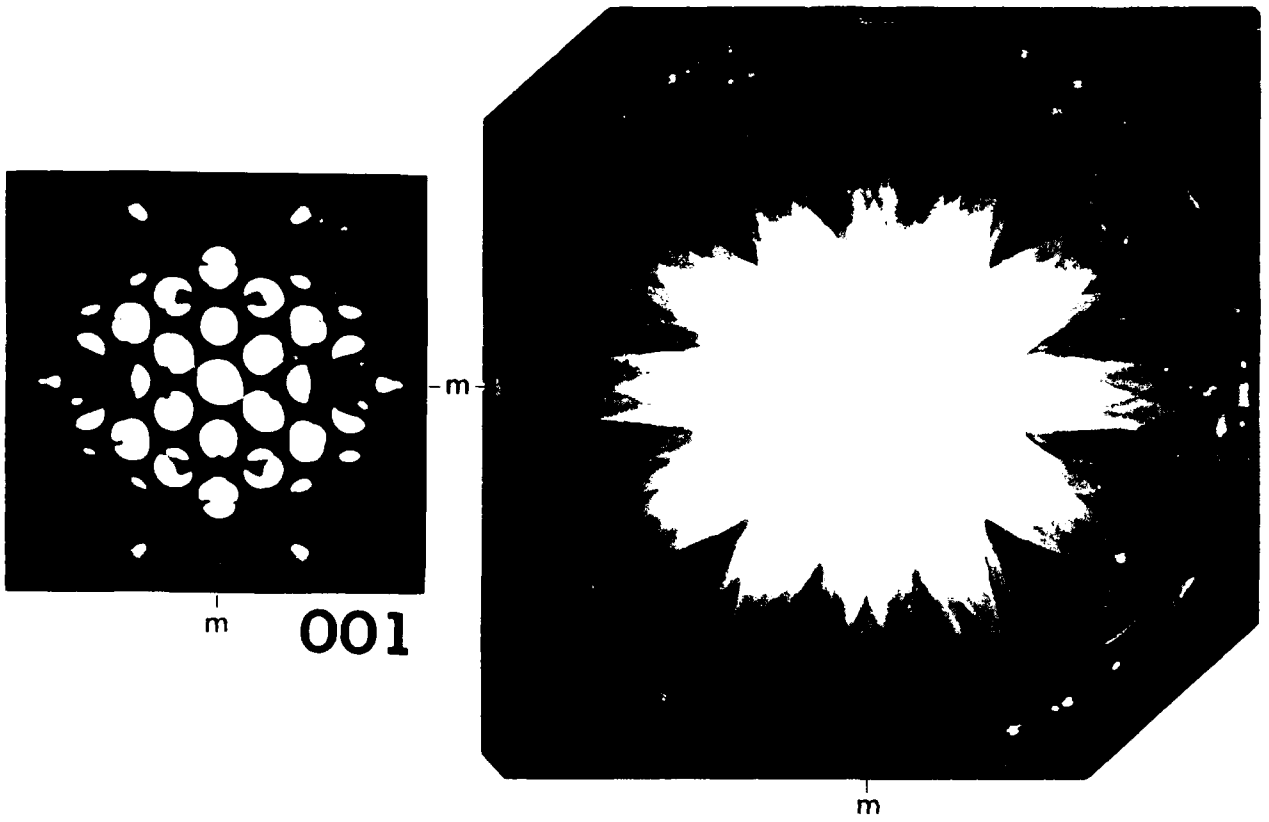

Figure 11 Convergent beam patterns (CBPs) from the [001] zone of the orthorhombic phase that formed in the higher Nb alloys

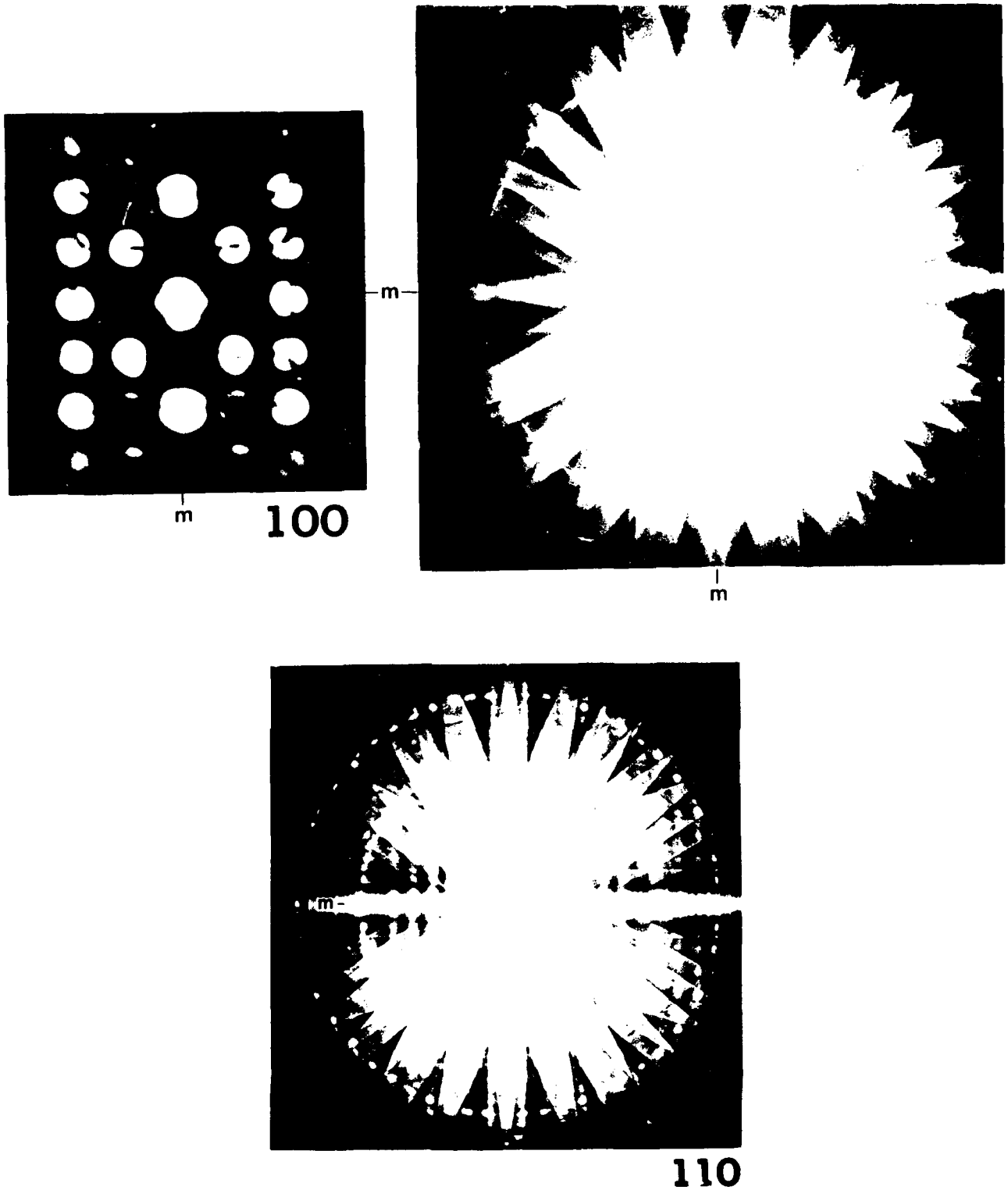

Figure 12 CBPs from the zone axes in the O-phase approximately parallel to the $<11\bar{2}0>$ poles of the α_2 phase: (a) **B**=[100], (b) **B**=[110].

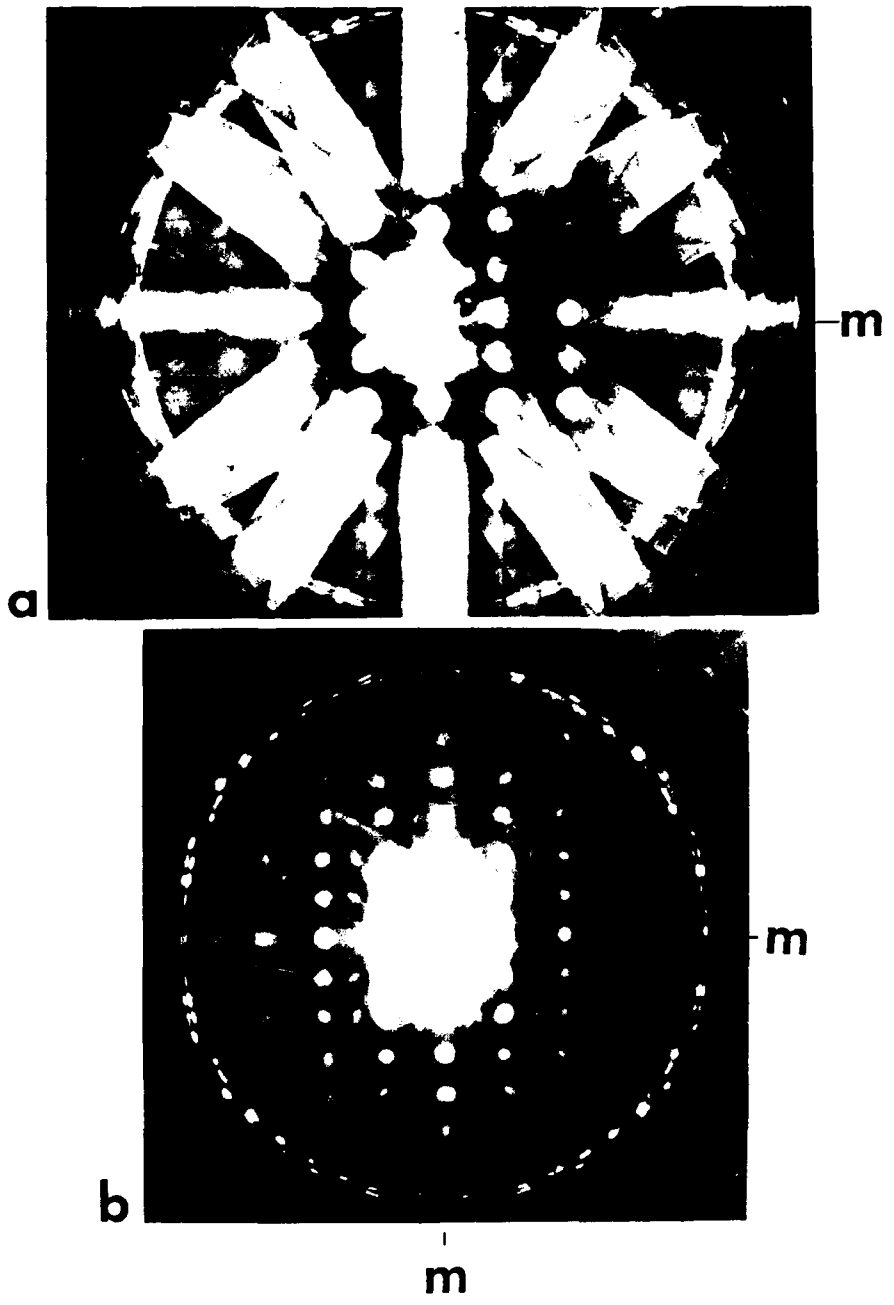

Figure 13 CBPs from the [010] which lies approximately parallel to the [1$\bar{1}$00] zone of the α_2 phase: (a) large convergence angle; (b) small convergence angle

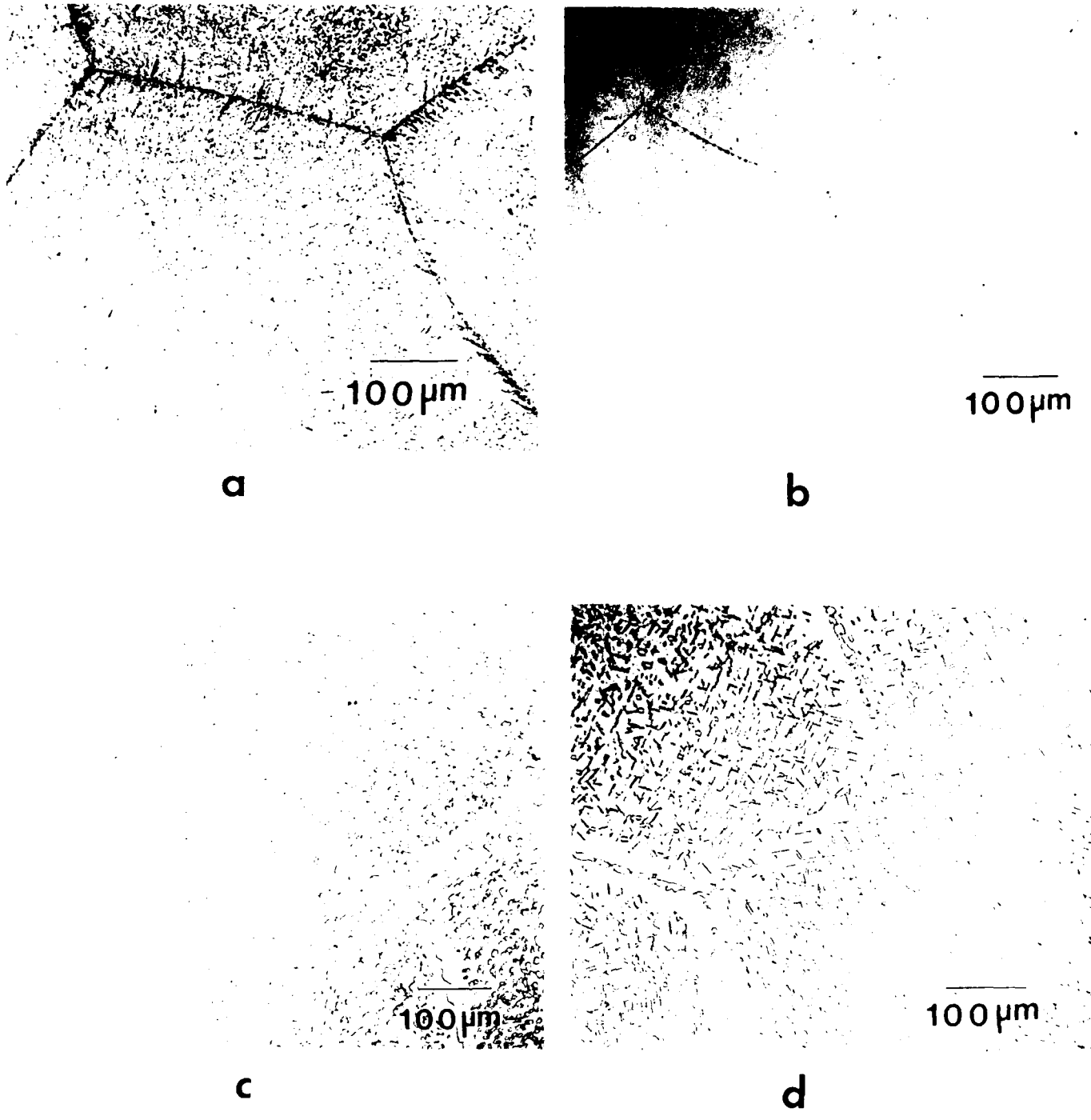

Figure 14 Optical micrographs of the 24-11 alloy solution annealed at 1250°C (2282°F) for 4h, water quenched, re-aged at the temperatures listed below and water quenched . (a) as-solution annealed;C (b) 1200°C (2192°F), 4h; (c) 1150°C (2102°F), 4h; (d) 1100°C (2102°F), 4h; (e) 1000°C (1832°F), 4h; (f) 900°C (1652°F), 24h; (g) 800°C (1472°F), 24h.

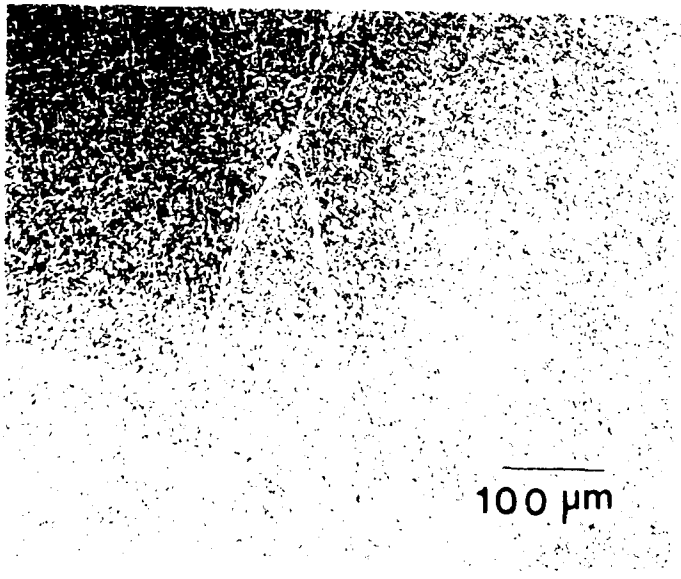

e

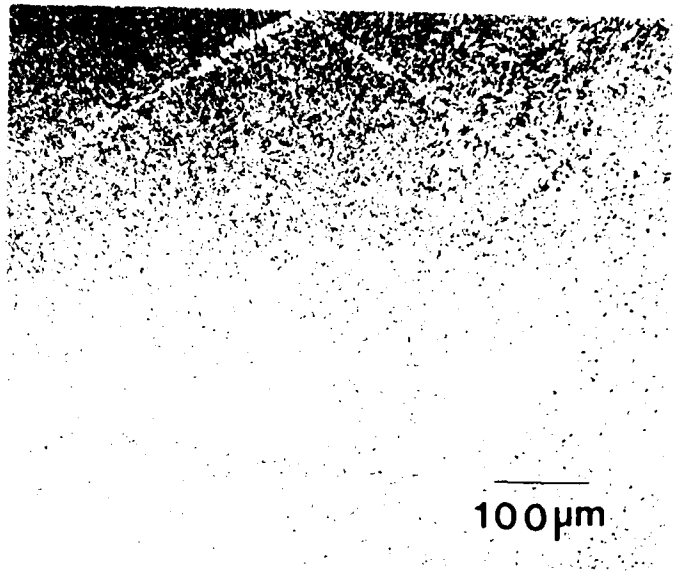

f

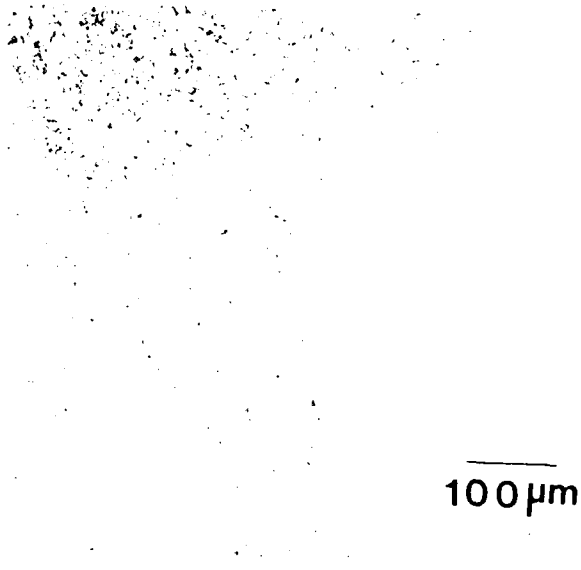

g

Figure 14 Optical micrographs of the 24-11 alloy solution annealed at 1250 C (2282 F) for 4h, water quenched, re aged at the temperatures listed below and water quenched . (a) as solution annealed;C (b) 1200 C (2192 F), 4h; (c) 1150 C (2102 F), 4h; (d) 1100 C (2102 F), 4h; (e) 1000 C (1832 F), 4h; (f) 900 C (1652 F), 24h; (g) 800 C (1472 F), 24h.

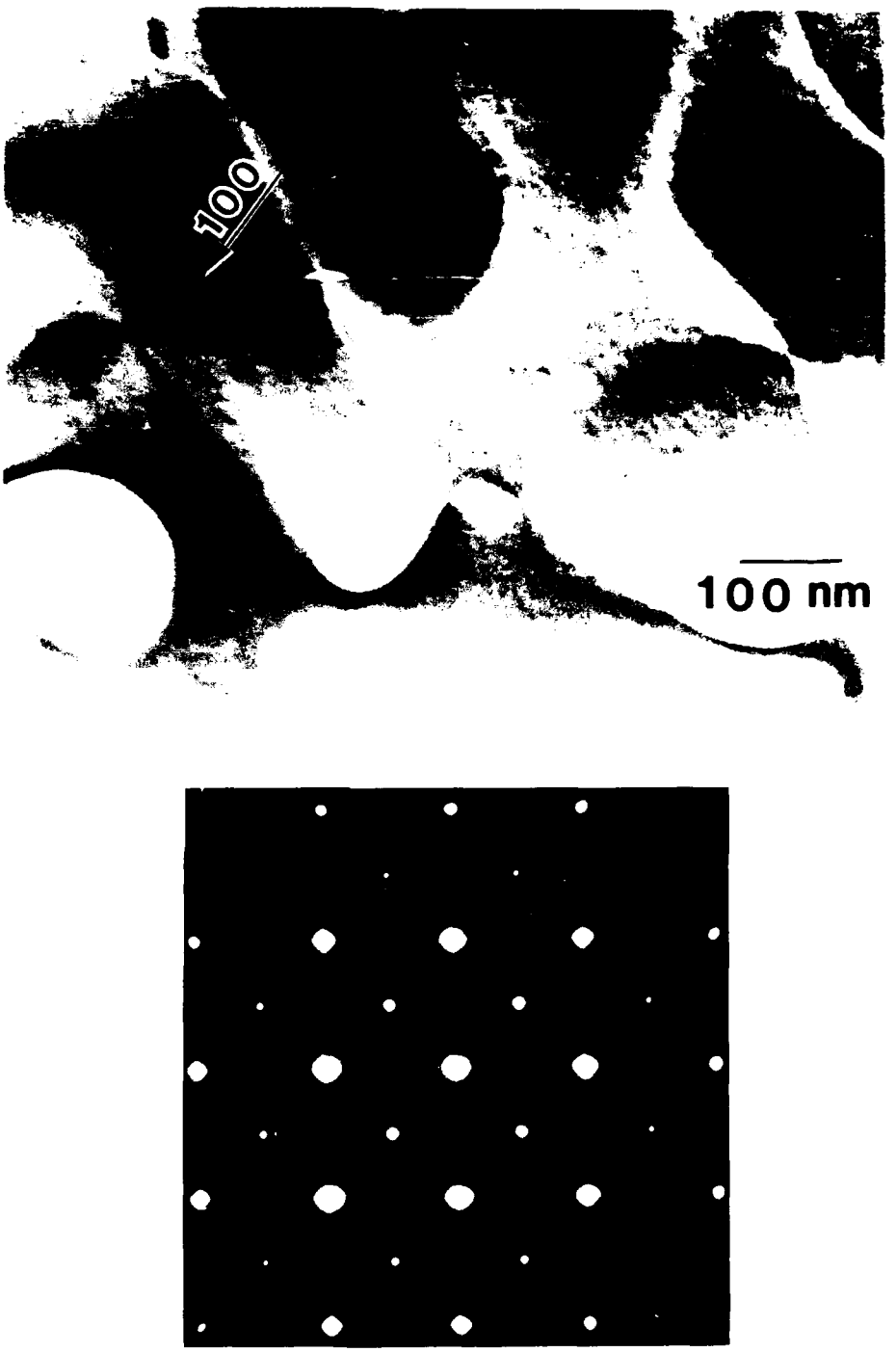

Figure 15 DFTEM (g=100) and SADP (B=[001]) of the B2 phase in the 24-11 alloy after annealing at 1200°C (2192°F) for 4 h and water quenching.

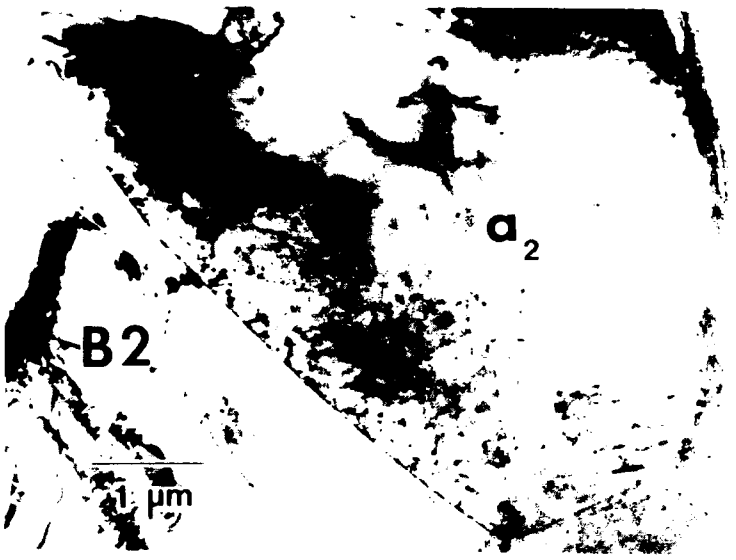

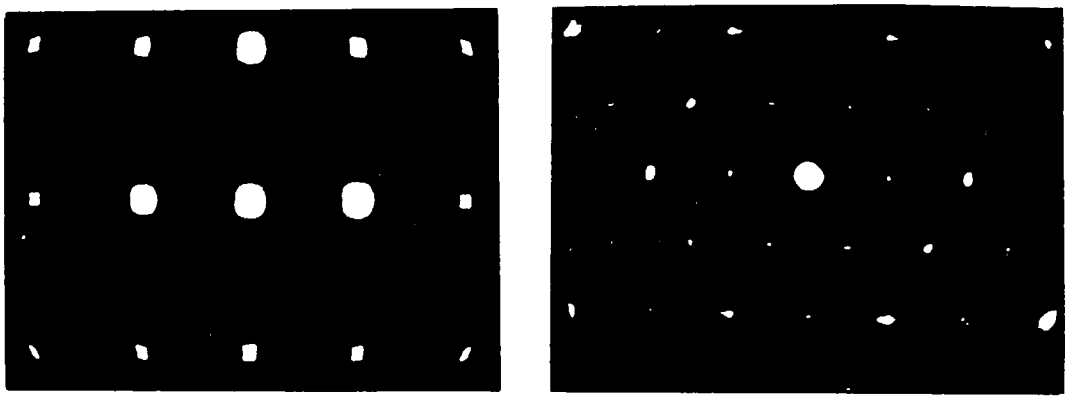

Figure 16 BFTEM and SADPs of the as-received 24-11 alloy after heat treating at 1000°C (1832°F) for 4h. The structure consists of both B2 and α_2.

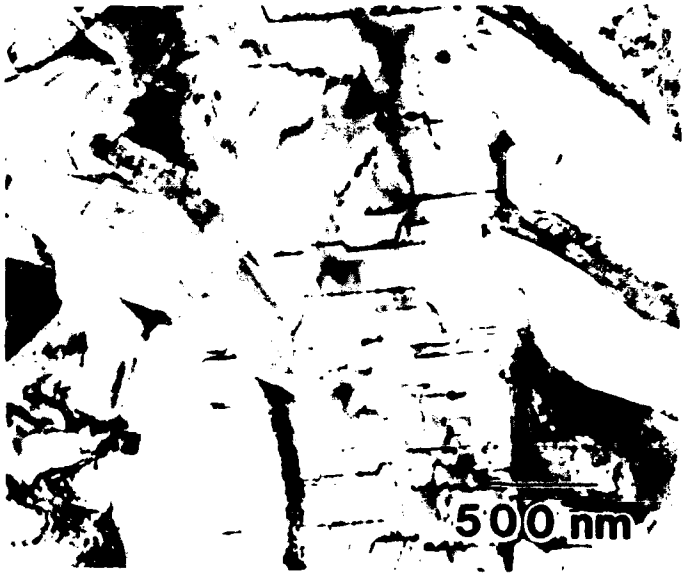

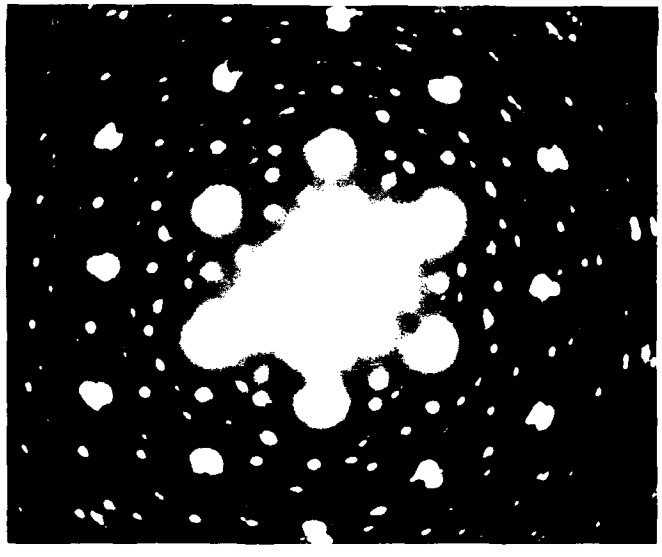

Figure 17 BFTEM and SADP of the 24-11 alloy after the 800°C (1652°F) anneal. The structure appeared to contain ~100% α_2.

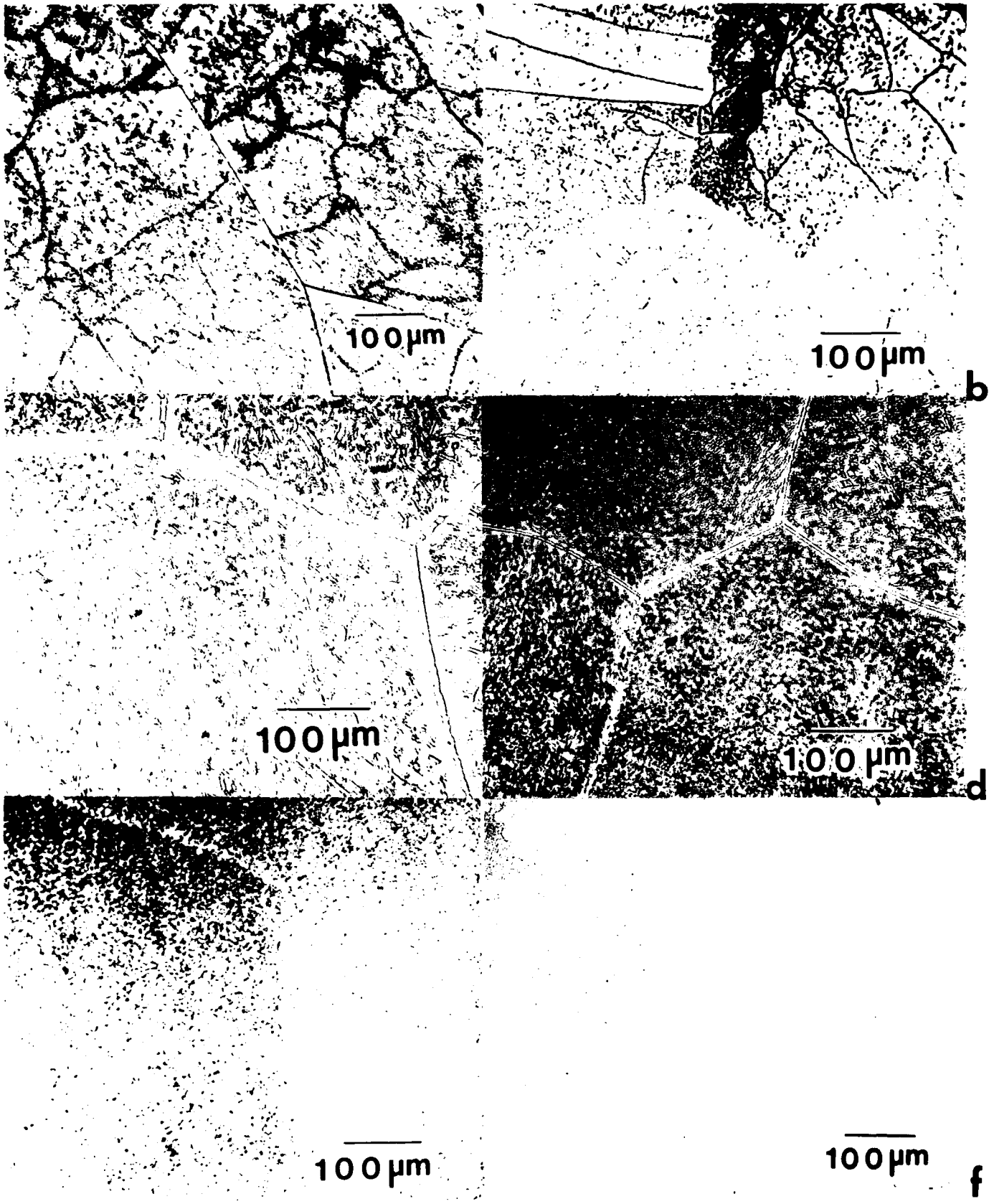

Figure 18 Optical micrographs of the 20Nb alloy, solution annealed at 1250°C (2282°F) for 4h, water quenched, re-aged at the temperatures listed below and water quenched. (a) 1250°C (2282°F), 4h; (b) 1200°C (2192°F), 4h; (c) 1100°C (2012°F), 4h; (d) 1000°C (1832°F), 4h; (e) 900°C (1652°F), 24h; (f) 800°C (1472°F), 24h.

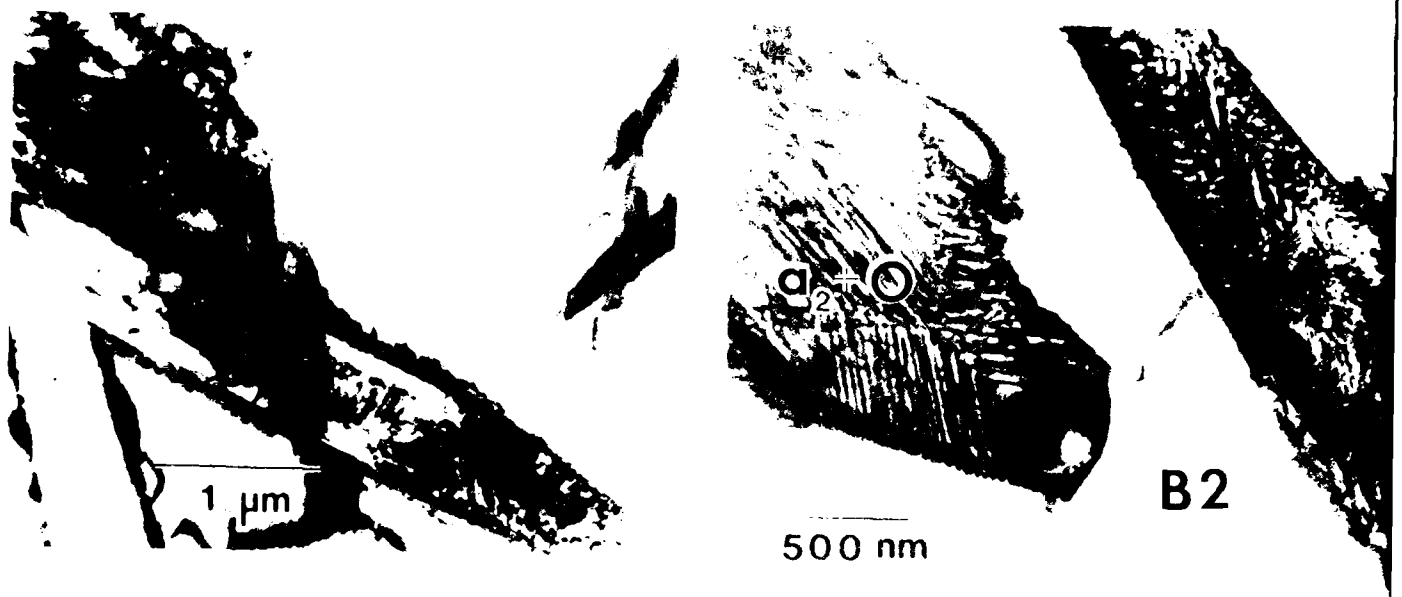

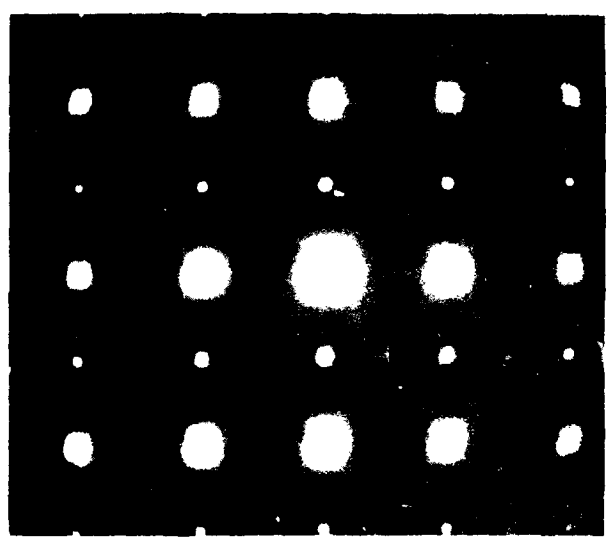

Figure 19. BFTEMs and SADP: B [illegible] heating at 1000°C (2012°F) for 3

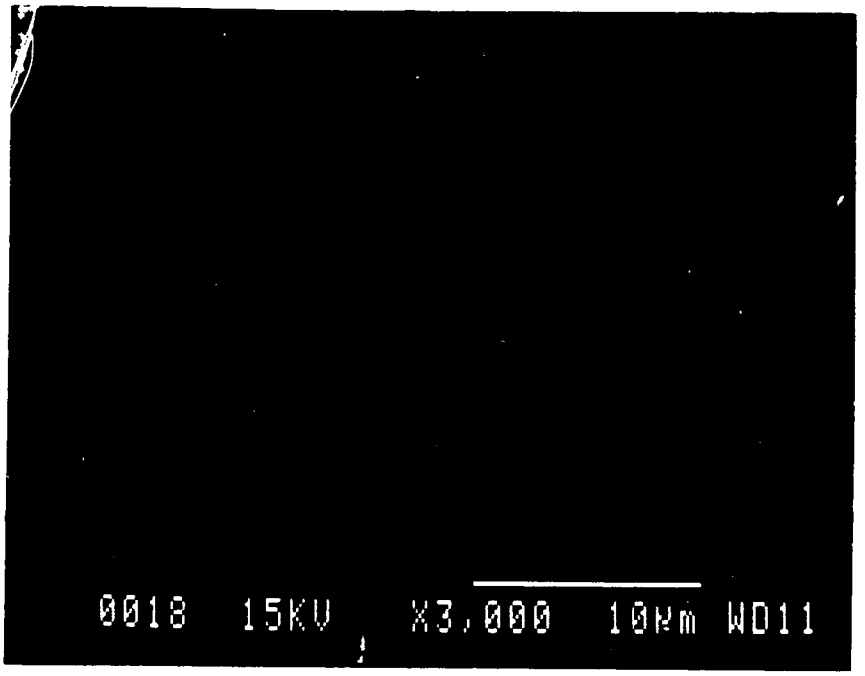

Figure 20 Back-scattered electron image of the 20Nb alloy after heat treating at 900°C (1652°F) for 24h.

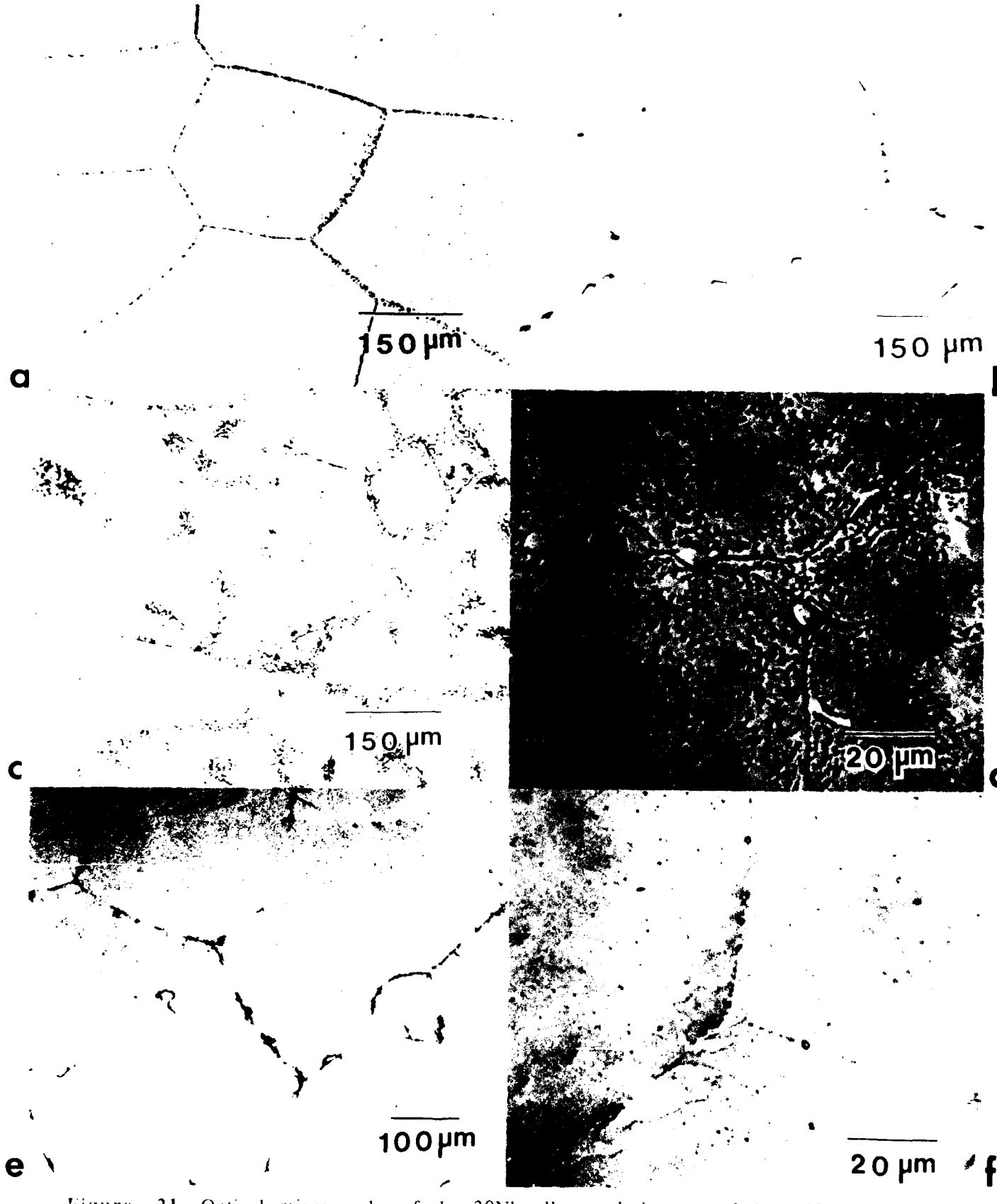

Figure 21 Optical micrographs of the 30Nb alloy, solution annealed at 1250°C (2282°F) for 4h, water quenched, re-aged at the temperatures listed below and water quenched (a) 1250°C (2282°F), 4h; (b) 1200°C (2192°F), 4h; (c) 1100°C (2012°F), 4h; (d) 1000°C (1832°F), 4h; (e) 900°C (1652°F), 24h; (f) 800°C (1472°F), 24h.

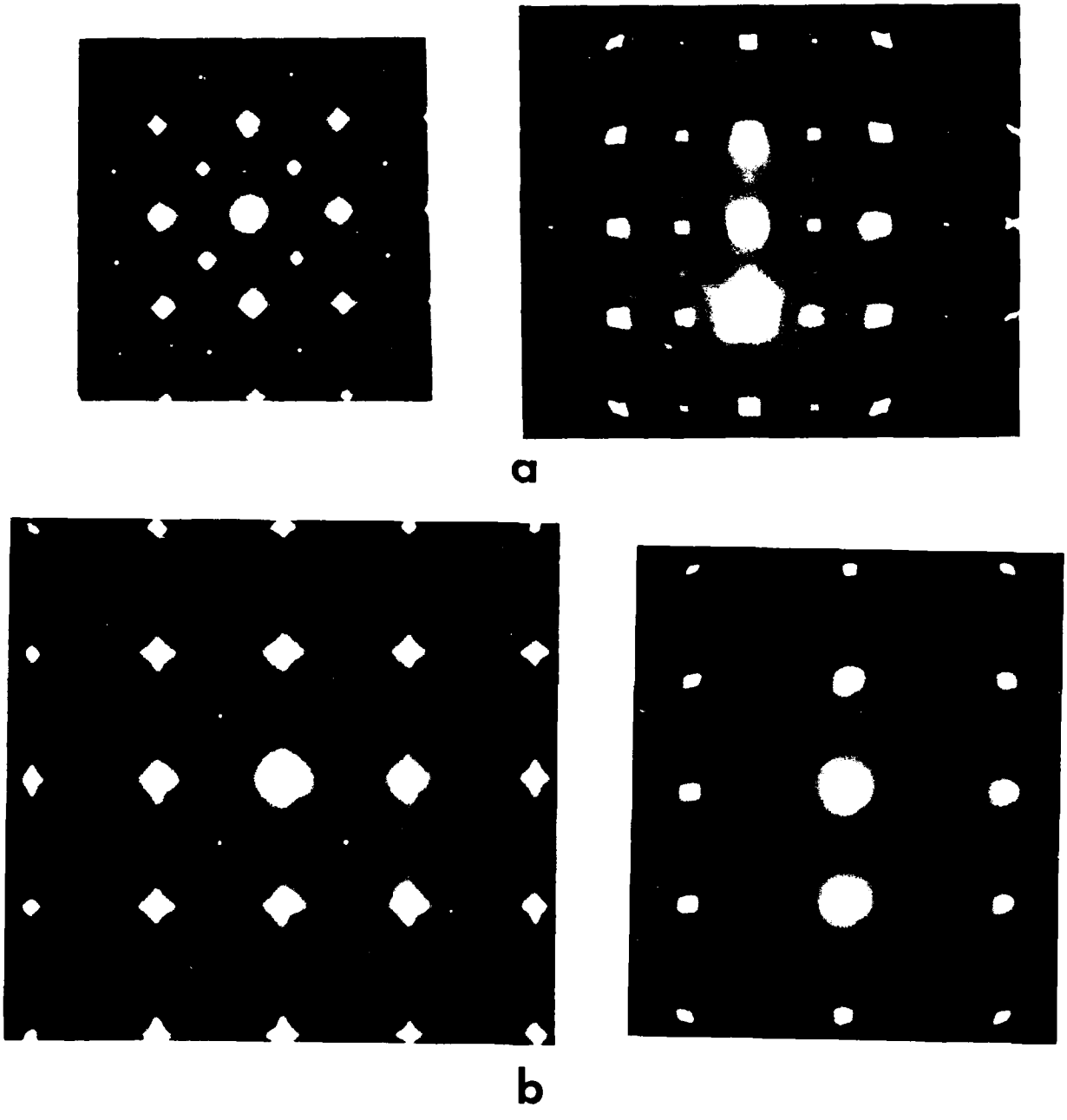

Figure 22 SADPs (B=[001] and [011]) from (a) as-RS splats and (b) heat treated bulk materials of Ti_3Al+30Nb. Note the differences in intensities of the B2 superlattice reflections.

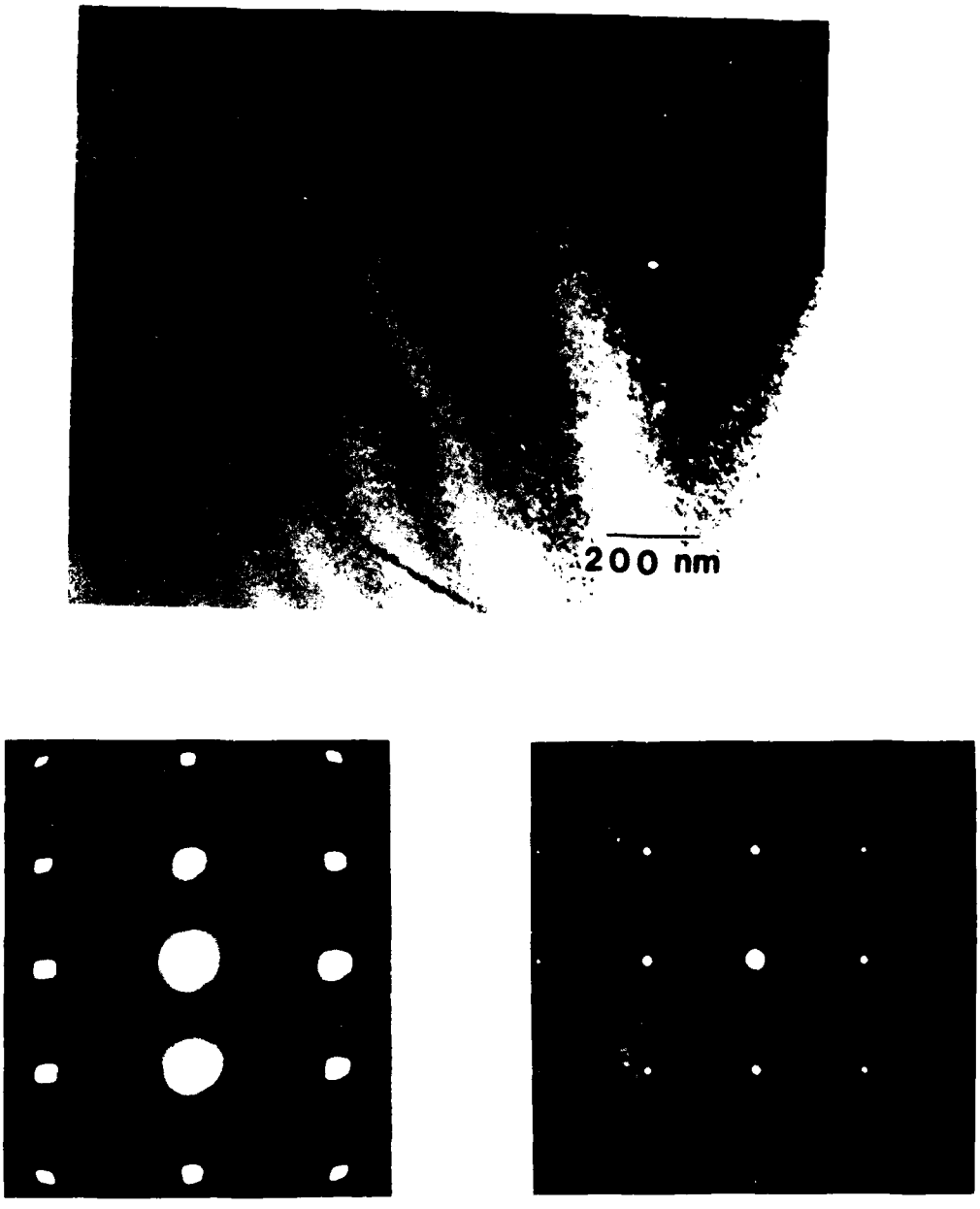

Figure 23 BFTEM and SADPs (B=[011] and [001]) of the 30Nb alloy after heat treating at 1200°C for 4h.

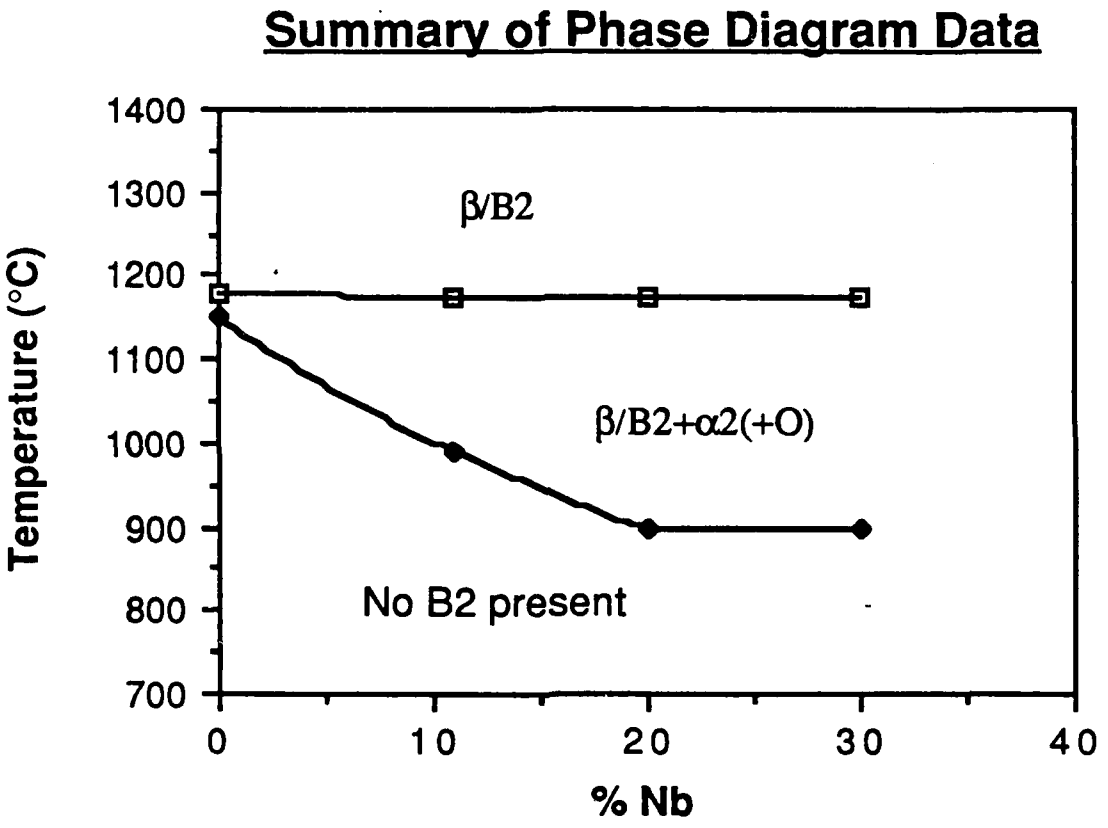

Figure 24 Temperature-composition diagram summarizing the results of the present study.